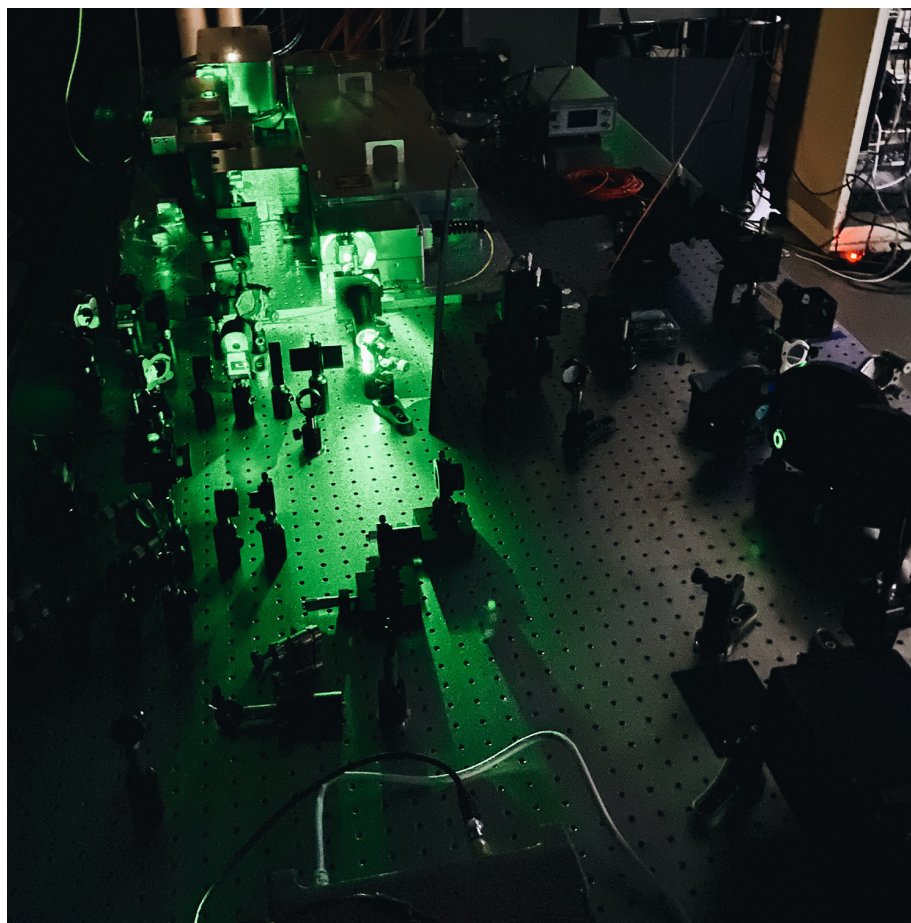




Exploring High Energy States in NV-Centers:  
Photoluminescence in Single-Point Defects in Diamonds  
Experimental Techniques  
Hasselt University - Ba2 Physics 2022-2023



Adam Blazejczak (1030499), Burak Kucuktopal (2158054)

May 2023

# Contents

<b>1 Abstract</b>	<b>3</b>
<b>2 Introduction</b>	<b>3</b>
2.1 Point defects in diamond . . . . .	4
2.2 NV-centers behavior at high laser powers . . . . .	4
<b>3 Theory</b>	<b>5</b>
3.1 NV-centers . . . . .	5
3.1.1 Geometry . . . . .	5
3.1.2 Photo-physical properties . . . . .	5
3.1.3 Photoluminescence spectrum . . . . .	6
3.1.4 Manipulating spin state with microwaves . . . . .	7
3.1.5 Rabi oscillations . . . . .	8
3.2 Einstein coefficients . . . . .	8
3.2.1 Spontaneous emission . . . . .	8
3.2.2 Absorption . . . . .	9
3.2.3 Stimulated emission . . . . .	9
3.3 Saturation curves . . . . .	9
3.3.1 Five level system . . . . .	10
3.4 Six level system of NV center . . . . .	12
3.4.1 Dynamics of the six-level system . . . . .	13
3.5 Density of states . . . . .	14
<b>4 Experimental setup</b>	<b>15</b>
4.1 NV-center sample . . . . .	16
4.2 Main procedure to find a NV-center . . . . .	17
4.2.1 Labview program: the 'Kernel' . . . . .	17
4.2.2 Rough alignment of the sample . . . . .	17
4.2.3 Mapping of inner-diamond surfaces using the confocal setup . . . . .	17
4.2.4 Finding the brightest spot . . . . .	17
4.2.5 Using ODMR to find a NV-center . . . . .	18
<b>5 Experimental Results and Discussion</b>	<b>18</b>
5.1 Finding and verifying NV-centers . . . . .	19
5.1.1 ODMR Spectrum Analysis . . . . .	20
5.1.2 Frequency Spectrum Analysis . . . . .	21
5.2 PL / PC dependence on applied voltage . . . . .	21
5.2.1 Voltage Sweeps . . . . .	22
5.2.2 Point of Interest . . . . .	24
5.2.3 Revealing ODMR and Rabi Oscillations at different voltages . . . . .	27
5.3 Saturation curves, $k_8$ and asymptotic behavior . . . . .	29
<b>6 Conclusions</b>	<b>32</b>
<b>7 Acknowledgements</b>	<b>32</b>
<b>8 Appendix</b>	<b>34</b>

# 1 Abstract

NV point defects in diamonds have been studied extensively in literature, initially using low laser powers and the four-level model [1]. However, recent investigations by Ádám Gali through ab initio calculations in higher power regimes introduced a fifth level [2], to consider state switching between the  $NV^-$  and  $NV^0$ . The theoretical model initially predicted zero photoluminescence (PL) at high laser powers, but ongoing experiments have indicated a possible high energy  $n_8$ -state, close to the conduction band, which would lead to non-zero asymptotic PL at high laser power. To shed light on this discrepancy, our research group modeled a NV-center with a six-level state, and derived a subsequent formula to calculate the population of the excited state at higher laser powers. Saturation curve measurements are obtained to study the validity and presence of this new high energy state. Setup refinements are required before making conclusions about the existence of state  $n_8$ .

During measurements, PL changes were observed due to changes in applied voltage on the sample. Investigation into PL dependence on potential has been investigated extensively using Optically Detected Magnetic Resonance (ODMR) and Rabi Oscillation, which confirmed initialization issues when cycling potential from non-zero to zero voltages, which is something researchers should be taking into account going into future research.

# 2 Introduction

Everyone in Western Culture is familiar with diamonds: it looks like a shiny crystal which is made out of billions of carbons, neatly arranged into a periodic arrangement, which lends a diamond her unique properties, e.g.: being one of the hardest material in the universe, being a highly transparent material to a broad range of frequencies (due to their large bandgap), being highly thermal conductive, and enjoying a high electric resistivity.

The carbon atoms within a diamond, responsible for these properties, are arranged into a highly specific lattice called a *diamond cubic* crystal structure, which repeats itself periodically across the whole volume of a diamond crystal. Such a diamond cubic structure can be seen in picture 1.

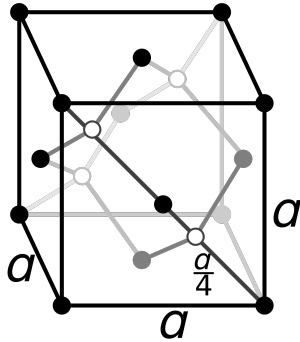


Figure 1: Carbon atoms arranged in a diamond cubic crystal structure

Diamonds are highly valuable, not only due to their high rarity, but also because of their applications in industries, and recently in quantum-based semiconductors research. In particular: diamonds, when embodying certain defects in their crystal structure, demonstrate interesting semi-conductor-like effects, like measuring magnetic fields[1], or manipulating spin-states[3], which are only explainable with modern quantum mechanics. As such, diamond-defects are currently paving the way for a whole new industry of quantum sen-

sors, quantum computing (Quantum RAM), and perhaps most important of all: a deeper understanding of matter at a quantum-level.

What follows is a discussion of a particular diamond defect: single point defect, and more particularly NV-centers (section 2.1). After that an introduction follows to justify the tone and experiments done in this research (section 2.2).

## 2.1 Point defects in diamond

When diamonds are grown in laboratory conditions for semiconductor research, an engineer is able to introduce extra non-carbon-atoms in the incubator's atmosphere. Under optimal thermodynamic conditions these non-carbon atoms (like Nitrogen, Germanium, or Silicon) join the crystal-structure of a diamond, which cause defects in the diamond's perfect cubic crystal structure.

Consider these defects as an absence of a carbon-atom, or replacement of a carbon-atom with another suitable atom (any atom from Group 4 could do [4]), in a location where usually a carbon-atom would be sitting in a diamond's crystal structure.

A *point-defect* is thus a location within a diamond's crystal structure, where a carbon-atom went missing or was replaced by another atom. When such a point-defect is present, and take for example a Nitrogen-atom being the point-defect, it is usually paired with a *vacancy* next to it, which is a missing carbon atom in the lattice. This is due to how the orbital structure of Nitrogen arranges itself within the crystal lattice, naturally causing the vacancy to emerge during the growth process of a diamond. Such a point-defect is called a Nitrogen-Vacancy Center, or in short an *NV-Center*.

Point-defects concerning other atoms (like Silicon, or Germanium) exist too, and they have each their own vacancy structures. E.g. in the case of GeV-centers (Germanium), two adjacent vacancies are present in the crystal structure of the diamond.

What's most interesting, and it's the main reason why the terminology above is being used, is the fact that the point-defect with adjacent vacancies are quantum mechanically equivalent to being a single system, i.e.: NV-centers operate as if they're made of a single Nitrogen-atom, namely the point defect itself (Nitrogen), without any trouble from first principle calculation. The same applies to GeV or PbV centers, though they exhibit multiple adjacent vacancies, the vacancies and point defects act like a single quantum system.

NV-center have photoluminescent properties when lasers at particular wavelength and laser power are focused on an NV-center. These properties get progressively more fascinating as one introduces other controlled variables to the environment, like the application of a microwave, magnetic field, or potential. In the theory section several of these topics are discussed in depth.

## 2.2 NV-centers behavior at high laser powers

To bring our introduction to a focal point, reasons for our chosen title and experiments are explained. The Photonics Department at IMO-IMOMEC is currently investigating the existence of a new high-level energy state which is close to the conduction band of an NV-center. This report focuses on performing experiments to investigate this new high energy state (called state  $n_8$ , see section 3.4) by performing saturation curve measurements. Results of our exploration can be found in section 5.3. During experiments it came to light that photoluminescence (PL) of an NV-center changes when one applies a varying voltage. To investigate possible changes in the crystal lattice environment, voltage sweeps experiments are conducted at different applied microwave wavelengths and laser

powers. Further, ODMR and Rabi Oscillation measurements are performed at various voltage sweeps to bring initialization issues to light. Results, and a progressive description through the many conducted experiments are described in section 5.2.

## 3 Theory

### 3.1 NV-centers

#### 3.1.1 Geometry

Nitrogen has 5 valence electrons. When a nitrogen-atom is introduced in a diamond lattice, three electrons form a covalent bond with their neighbouring carbon atoms, having a pair electrons remaining, often called a *lone pair*[5]. The vacancy on the other hand is considered to exhibit three electrons (remember - it's actually a missing atom!), two of them form a covalent bond with their neighbouring carbon atoms. This electronic structure results in a spacial arrangement conform to the trigonal pyramidal geometry( $C_{3V}$ ), in accordance to Valence shell electron pair repulsion theory(VSPER). In figure 2 an image of this geometry can be seen.

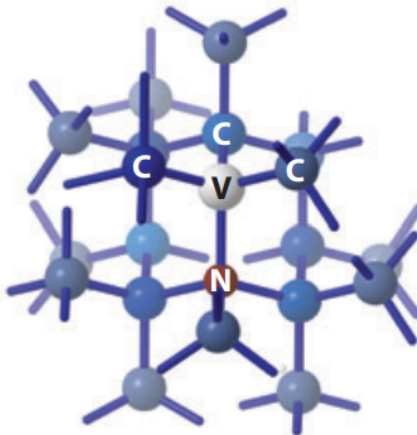


Figure 2: Geometry of the NV-center[6]

In case of the neutral  $NV^0$  center, there is an exchanging/swapping between the electron of the vacancy that is unbound and the other covalently bounded electrons. This vacancy is not of interest in semiconductor research, as it exhibits no magneto-optic effects[6]. The one that has magnetic characteristics is that of the negatively charged NV-center ( $NV^-$ ). This center is also used in our experiments.

#### 3.1.2 Photo-physical properties

There are different models to try to explain the NV-center. In this thesis we will state the fundamentals with the model proposed by L. Rondin, J.-P. Tetienne, T. Hingant, et al. in the paper *Magnetometry with nitrogen-vacancy defects in diamond*[7]. The NV-center has contained four energetic levels inside the *bandgap* of the diamond, thus naming it a *four-level system*. The first being the ground state, which we'll refer to as  $|g\rangle$ .

The ground state is a triplet one (Total Spin  $S=1$ ), meaning that there are 3 spin projections present, the degenerate ones:  $m_s = \pm 1$  and the non-degenerate  $m_s = 0$ .

The  $m_s = \pm 1$  and the  $m_s = 0$  have different energy levels due to their *spin-spin interactions*. Their difference in energy, also referred to as the zero(magnetic)-field-splitting,

is given by  $D=2.87\text{GHz}$  (see figure 3). The degenerate case can be made non-degenerate by applying a magnetic field, essentially splitting the energetic levels into their spin-up and spin-down counterparts (Zeeman effect). In fact, this technique is used to utilize an NV-center as a magnetic-sensor, however the discussion of this application falls out of the scope of our discussion. To readers who'd like to dive into this, we refer to [1].

The symmetry that is associated with the ground state is  ${}^3A_2$ . The three refers the number of projections and  $A_2$  to the Coxeter symmetry group. This group is isomorphic (i.e. algebraically equivalent) to the dihedral group  $D_{2,3}$ , meaning it exhibits the same rotations and reflections inherent to that of an equilateral triangle. Note that both groups are non-commutative, which is why NV-centers can be characterised within a certain diamond (i.e. determine the average direction of present NV-centers).

The second energy state of an NV-center is the excited state, denoted as  $|e\rangle$ . This state is also a triplet state (total spin  $S=1$ ) and has a Zero-field-splitting of  $D = 1.42\text{GHz}$ , with again a degeneracy at  $m_s = \pm 1$  (we refer to figure 3). This state has a symmetry group of  ${}^3E$ .

The third and fourth state are  ${}^1E$  and  ${}^1A_1$ , but both having different energies. These two are respectively the excited and ground state of the so-called metastable state  $|s\rangle$ <sup>[7]</sup>

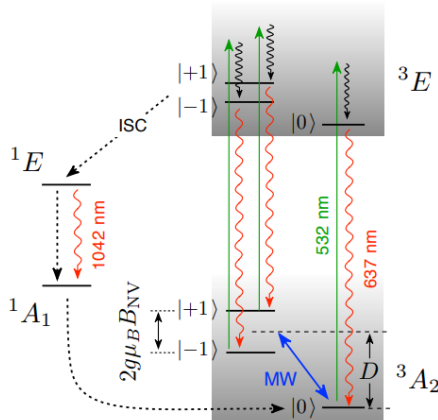


Figure 3: Energy four level structure of NV-center. The splitting of the degenerate energy levels  $m_s = \pm 1$  is due to an applied magnetic field. Note: transitions which aren't spin conserving are not represented due to its lower probability.[7]

### 3.1.3 Photoluminescence spectrum

In our experiments, which are explained in section 4 about the experimental setup, an NV-center (a quantum system) is excited by means of a laser operating at a wavelength under emission wavelength(637 nm) to excite NV centers from the ground to the excited state.[5]. We will use as excitation wavelength range: 540nm - 570nm

As the electrons within an NV-center are excited, the NV-center enter a higher energy state. After some time the quantum system will experience a form of relaxation in an attempt to return back to its ground (and stable) state.

This can occur either through radiative means (energy is released via photon emission) or

---

<sup>1</sup>Note that in some papers, these two symbols are interchanged. We'll take over the notation given by L. Rodin et al.

non-radiative means (energy is released through vibrational or kinetic means, i.e. phonons). The *path of relaxation*, through the various energy levels is what drives this research, and makes this experiment very interesting. For example: some transitions of the NV center are forbidden, while others are forced to occur via radiative means, or via intersystem crossing(ISC), see figure 4.

If a NV center arrives in the excited state  $|e\rangle$  by the laser, the NV center can transition directly to its lowest (ground) state without any associated phonon emission. The energy dissipation occurs purely via emission of photons, which can be captured as a peak at 637nm [7] on the Photoluminescence (PL) Spectrum (figure 3), which is called the Zero-Phonon-Line (ZPL).

However, only a small population of produced photoluminescence will be found in the Zero-Phonon-Line. Many relaxations will occur at a higher wavelength due to the presence of vibrational relaxations. When these relaxations happen, a part of the energy from the excited state  $|e\rangle$  to the ground state  $|g\rangle$  will be lost. As a consequence, the photons that are emitted have a lower energy than that of the photons from the (ZPL). Because the wavelength is inversely proportional to the energy of a photon, it follows that the wavelength of every other photon not contained in the ZPL, is larger. Due to this, we observe an increased PL in the range 630nm – 800nm called the *phonon wind* when measuring the PL-spectrum of a NV center, see figure 4.

The NV-center can also go via non-radiative interstate crossing (ISC) into  $^1E$  of the metastable state  $|s\rangle$ . The center will relax into the  $^1A$  state, emitting infrared light with a wavelength equal to 1042 nm(see figure 1), whereafter it will end up in the ground state.

This ISC is helpful when manipulating the spin of the NV-center using microwaves.

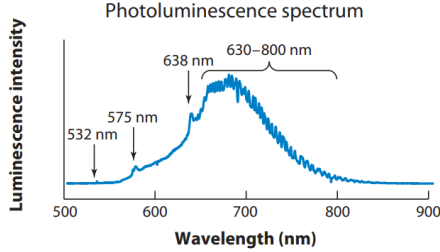


Figure 4: Characteristic PL-spectrum of a NV-center[6] with a peak at 638nm and a wide phonon sideband from  $\approx 630\text{nm}-800\text{nm}$

### 3.1.4 Manipulating spin state with microwaves

One can measure spin-properties and energy structures of NV-centers using Electron Paramagnetic Resonance-spectrum analysis. Since the optical transitions of the NV-centers are strongly spin-conserving, there can measured the resonant absorption of microwave radiation by the unpaired electron in the NV-center using an EPR-spectrum.

By applying a microwave at  $f = 2.87\text{GHz}$ , the NV centers in the  $m_s = 0$  (ground state) can be flipped into the  $m_s = \pm 1$  state, which will cause a higher population of  $m_s = \pm 1$  in the excited state  $|e\rangle$  after excitation by a laser. Thus the ISC is more probable, resulting in more infrared light being emitted, and less red light being emitted from ZPL, which characterizes the dip on the EPR spectrum (see figure 5).

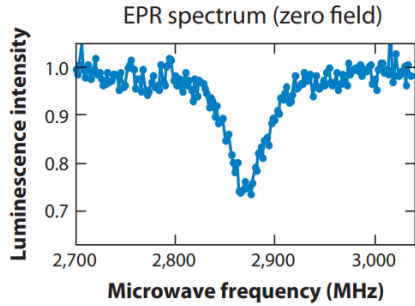


Figure 5: EPR-spectrum of NV-center in case of no magnetic field[6].

### 3.1.5 Rabi oscillations

When a driving field is being applied to a quantum two-level state, oscillations between the two states occur, also called Rabi oscillations. In the model of the NV center, the  $m_s = 0$  and  $m_s = \pm 1$  are the corresponding quantum two-level state. The driving field in this case is the microwave which is sent with pulses of length  $\tau$  and has a frequency close to the resonant frequency 2.87 GHz.

Rabi oscillations can then be used as another method of measuring ODMR if there is also use of pulsed laser signals with 'dark time'  $\Delta t$  the time between two pulsed laser signals and the pulsed microwave during in this dark time. At each laser pulse, we measure the PL and set this in function of the pulse length of the microwave. Normally this plot would give a non-damped sinusoidal form, but because of the presence of the other states, we will get a damping oscillatory behavior. The difference in PL between the first peak and the first dip, will give the contrast in the corresponding ODMR spectrum. Due to the presence of surrounding magnetic fields(such as the Earth magnetic field), the degeneracy of the  $m_s = \pm 1$  state can be lifted a little bit, resulting in a double Rabi oscillation, thus registering the sum of two sinusoidal signals. To solve this problem, we have also added an extra magnetic field such that we split it even more, having two individual sinusoidal signals and not a sum.

The theory of Rabi oscillations is not being discussed, since this falls out of scope of this thesis. For further reading, we suggest [8].

## 3.2 Einstein coefficients

The Einstein coefficients govern the rate at which the photonic processes absorption, spontaneous emission and stimulated emission occur. This will be important when we're dealing with the population dynamics of the proposed NV-models.

### 3.2.1 Spontaneous emission

The excited electrons in an atom have the tendency to fall back to its lower energy level, bringing the atom back to a more energy-stable state. Together with this relaxation, there is the emission of photons. The rate at which these photon emissions are occurring in a population of atoms  $N_2(t)$  is given by the Einstein A coefficient. The corresponding rate equation is given as:

$$\frac{dN_2}{dt} = -A_{21}N_2 \quad (1)$$

The index of the A coefficient refers to the probability that an atom in the excited state will fall into the ground state per unit time[8]. This could also be seen as the probability that there will be a photon emission per unit time, therefore this can be directly linked to the photoluminescence, see (3.2.3).

The A Einstein coefficient gives also rise to calculating the **radiative lifetime**, also called the **transition period** of an excited state:

$$\tau = \frac{1}{A_{21}}$$

### 3.2.2 Absorption

Absorption happens when an atom is being shone by a bundle of photons, giving the exact amount of energy to lift the population of atoms  $N_1(t)$  to a higher energy state  $N_2(t)$ . This photonic process is not spontaneous and is dependent on the wavelength,  $\lambda$ , of the bundle of photons. The absorption rate equation is given by[8]:

$$\frac{dN_1}{dt} = -B_{12}^\omega N_1 u(\omega) \quad (2)$$

$B_{12}^\omega$  is referring to the Einstein B coefficient [ $m^3 J^{-1} s^{-2}$ ], while  $u(\omega)$  [ $J m^{-3} s (rad)^{-1}$ ] is the spectral energy density of the electromagnetic field.

### 3.2.3 Stimulated emission

There is also another type of emission, by which a population of atoms in an excited state  $N_2(t)$  can be relaxed by firing it with a bundle of photons with a angular frequency around  $\omega$ . The rate equation is given by:

$$\frac{dN_2}{dt} = -B_{21}^\omega N_2 u(\omega) \quad (3)$$

These rate equations can be also seen as the rate of emission per unit time, giving following relation with the photoluminescence, PL, of a certain atom:

$$PL \propto B_{(ij)}^\omega N_i \quad (4)$$

with  $i, j \in \{1, 2\}$ ,  $i \neq j$  and  $B_{(ij)}^\omega$  the Einstein coefficient of the corresponding photonic process.

## 3.3 Saturation curves

The saturation curves of a NV center are the curves we obtain when we plot the photoluminescence, counts/s, of the center in function of the laser power, in mW. As stated earlier, there are different models used to described NV centers. In section 3.1.2 about the photo-physical properties, we introduced the four-level system to be able to state in a simple fashion the basic properties of the NV center. The ab initio calculations by Ádám Gali from the Hungarian Academy of Sciences[2] together with the more recent paper on exploiting the ionization dynamics in nitrogen vacancy[9] made us think to improve to the four level system as represented in figure 6 to account for the  $NV^- \rightarrow NV^0$  transition. But this transition would only be more probable to happen once we are in a high power regime and would be seen separately from that of the  $NV^-$  when the laser power is too low ( $< 2mW$ )[9].

But this five-level system doesn't seem to be enough as will be seen in the following section: it will be shown that if we would adapt this new model, there will possible be a problem with the saturation curves' behaviour for big laser powers. We will propose a model to try to resolve this.

### 3.3.1 Five level system

Our research group initially represented a NV-center by a five-level system, four given by figure 3, while the fifth is the transition from which the  $NV^-$  center goes from the excited state to a  $NV^0$ . This is represented by figure 6.

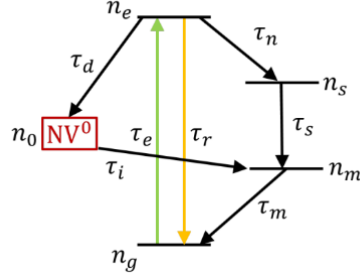


Figure 6: Traditional energy representation of a NV center as five level system[8,9]. The  $\tau'_i$ 's represent the *transition period*[10], while the  $n'_i$ 's are representing the population at each state[6].

The population of the five levels of the NV center are defined as 0 being empty and 1 being fully populated. The letters for the different population levels are as follows:

- $n_g$ : population of the ground state.
- $n_e$ : population of the excited state.
- $n_0$ : population of the  $NV^0$  state.
- $n_s$ : population of the singlet state.
- $n_m$ : population of the metastable state.

Because we are working with the stimulated processes, absorption and stimulated emission will be the most interesting to talk about. These two transition occurring between the different levels can be characterized by the *transition rate*  $k$ , which corresponds with the Einstein coefficients times the spectral energy density discussed in section 3.2. For each Einstein coefficient one could define the transition period,  $\tau = k^{-1}$ . The different transition times in our four level system are:

- $\tau_d$ : this is the deionization transition time.
- $\tau_i$ : the ionization transition time.
- $\tau_e$ : the excitation transition time.
- $\tau_r$ : the radiative transition time.
- $\tau_n$ : the non-radiative transition time.
- $\tau_s$ : the singlet transition time.
- $\tau_m$ : the metastable transition time.

To make an appropriate fit, we first would need to determine theoretically how the saturation curve would look like. The main radiative process is given by the transition from  $n_e \rightarrow n_g$ , the metastable state transition  $\tau_s$  will also radiate infrared light, but this has a too high wavelength to fall in our active PL measurement frame(580nm – 1000nm), therefore we can only consider the radiative process coming from the transition  $n_e \rightarrow n_g$ . From equation (4) it follows:

$$I \propto \frac{dn_e}{dt} = k_r \cdot n_e \quad (5)$$

So once  $n_e$  is known in detail, we could approximate the laser-power dependent k's as being proportional to the laser power by comparing the units of power( $\text{Watt} = \text{Js}^{-1}$ ) and the spectral density( $J^{-1}\text{m}^{-3}\text{s}(\text{rad})^{-1}$ ). Thus  $k(P) = aP$ , with  $P$  the power of the laser in  $W = \text{Js}^{-1}$  and  $a \in \mathbb{R}$  having units  $(\text{J})^{-1}$ . With this, we can find the behavior of the saturation curve using the concept of *density of states*. The dynamics of the five level system Every transition from a state  $n_i \rightarrow n_j$  creates a *population flux*  $\frac{dN}{dt} = n_i k$ . If there is a steady state, the net population flux must be zero everywhere, resulting in the following set of equations describing the dynamics of our five level system:

$$\begin{cases} 0 = \dot{n}_g = n_e k_r + n_m k_m - n_g k_e \\ 0 = \dot{n}_e = -n_e k_r - n_e k_n + n_g k_e - n_e k_d \\ 0 = \dot{n}_0 = n_e k_d - n_0 k_i \\ 0 = \dot{n}_s = n_e k_n - n_s k_s \\ 0 = \dot{n}_m = n_s k_s - n_m k_m \\ \text{conservation of elements: } \sum_i n_i = 1 \end{cases} \quad (6)$$

There can be quickly seen that one cannot solve this highly non-linear set of equations by hand. Using program languages such as Python or Matlab to solve for  $n_e$ , didn't give anything either. This means that the set of equations are mathematically too rigid. To resolve this, one must be closer related to physical interpretations, rather than mathematically rigorous. There can be found an expression for  $n_e$  by using the method of *density of states*[10].

Using the method of *density of states*[10], we get:

$$n_e = \left(1 + \frac{\tau_e}{\tau_r} + \frac{\tau_i + \tau_e + \tau_m}{\tau_d} + \frac{\tau_m + \tau_e + \tau_s}{\tau_n}\right)^{-1} \quad (7)$$

Now that the expression for  $n_e$  is found, we could look at the behaviour for high powers. Experimentally, it is known that  $\tau_e, \tau_d$  and  $\tau_i$  are transition periods depending on the laser.

So by equation (5) we can rewrite these three in:

- $\tau_d = \frac{1}{k_d \cdot P}$
- $\tau_e = \frac{1}{k_e \cdot P}$
- $\tau_i = \frac{1}{k_i \cdot P}$

Filling this in (7):

$$n_e = \left(1 + \frac{1}{k_e \cdot P \cdot \tau_r} + \frac{\frac{1}{k_i \cdot P} + \frac{1}{k_e \cdot P} + \tau_m}{\frac{1}{k_d \cdot P}} + \frac{\tau_m + \frac{1}{k_e \cdot P} + \tau_s}{\tau_n}\right)^{-1} \quad (8)$$

Simplifying gives:

$$n_e = \left(1 + \frac{1}{k_e \cdot P \cdot \tau_r} + \frac{k_d}{k_i} + \frac{k_d}{k_e} + \tau \cdot k_d \cdot P + \frac{\tau_m + \frac{1}{k_e \cdot P} + \tau_s}{\tau_n}\right)^{-1} \quad (9)$$

If  $P \rightarrow \infty$ , the term  $\tau \cdot k_d \cdot P$  will be dominant resulting in:

$$n_e = (\mathcal{O}(P))^{-1} = \mathcal{O}\left(\frac{1}{P}\right) \quad (10)$$

Thus  $n_e \rightarrow 0$ , if  $P \rightarrow \infty$ . From equation (5):

$$PL \rightarrow 0, \text{ if } P \rightarrow \infty \quad (11)$$

This analysis shows that the population of excited states will go to zero for high laser powers, meaning that the metastable state  $n_s$  will be overpopulated. So if we'd take this model as reference, we'd expect that the PL, with an active measurement spectrum not measuring for infrared, will go to zero for high laser powers, which in this case would mean bigger than 20 mW.

The preliminary results of the research group we joined of the saturation curves for laser powers bigger than 20 mW seems to give some asymptotic behaviour, see figure 7. Therefore, to try to account for this by adding a new  $n_8$  state to the five-level state. The following section describes this new model, together with its predictions on high laser powers.

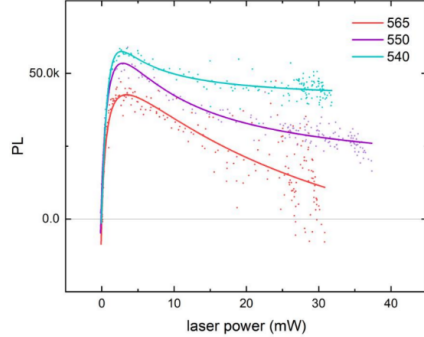


Figure 7: Examples of measurement the saturation curve for different wavelength, giving an asymptotic behavior.[11]

### 3.4 Six level system of NV center

The preliminary results of the saturation curve gave the idea of a sixth state called  $n_8$  which got activated once the laser power is high enough. This gives the following scheme:

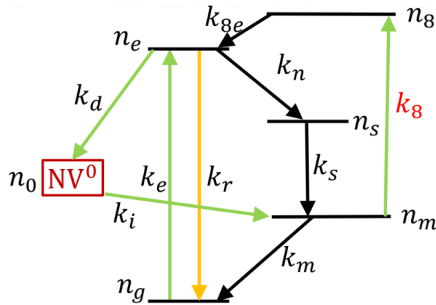


Figure 8: Six level system [10]

Here transition rates instead of the transition times are used to describe the transitions. The population of the new state is called  $n_8$  and the transition rate from  $n_m \rightarrow n_8$  is defined as  $k_8$ . While that from the new state to the excited state as the excited transition rate,  $k_{8e}$ .

### 3.4.1 Dynamics of the six-level system

We again could write down the system of non-linear equations describing the dynamics of the six level system:

$$\begin{cases} 0 = \dot{n}_g = n_e k_r + n_m k_m - n_g k_e \\ 0 = \dot{n}_e = -n_e k_r - n_e k_n + n_g k_e - n_e k_d + n_8 k_{8e} \\ 0 = \dot{n}_0 = n_e k_d - n_0 k_e \\ 0 = \dot{n}_s = n_e k_n - n_s k_s \\ 0 = \dot{n}_m = n_s k_s - n_m k_m - n_m k_8 + n_0 k_i \\ 0 = \dot{n}_8 = n_m k_8 - n_8 k_{8e} \\ \text{conservation of elements: } \sum n_i = 1 \end{cases} \quad (12)$$

But now the system is even more complex than that given in section 3.3.1, so we'll make again use of the method of density of states to get:

$$n_e = (1 + \sum_i \frac{t_i}{\tau_j})^{-1} = (1 + \frac{\tau_e}{\tau_r} + \frac{t_2}{\tau_d} + \frac{t_3}{\tau_n})^{-1} \quad (13)$$

Note that the route to go back to the excited state is not anymore uniquely defined, therefore  $t_2$  and  $t_3$  need to be acquired using the harmonic average since we're working with rates[12]. For  $t_2$  we have the route  $n_0 \rightarrow n_m \rightarrow n_g \rightarrow n_e \wedge n_0 \rightarrow n_m \rightarrow n_8 \rightarrow n_e$ , getting for the total times for each route respectively  $t_{21} = (\tau_m + \tau_e + \tau_i) \wedge t_{22} = (\tau_i + \tau_8 + \tau_{8e})$ , taking the harmonic average gives:

$$t_2 = \frac{1}{\sum_{i=1}^2 \frac{1}{t_{2i}}} = \frac{1}{\frac{1}{\tau_m + \tau_e + \tau_i} + \frac{1}{\tau_i + \tau_8 + \tau_{8e}}} = \frac{(\tau_m + \tau_e + \tau_i) \cdot (\tau_i + \tau_8 + \tau_{8e})}{(\tau_m + \tau_e + \tau_i) + (\tau_i + \tau_8 + \tau_{8e})} \quad (14)$$

In similar fashion, we can calculate  $t_3$ :

$$t_3 = \frac{(\tau_m + \tau_e + \tau_s) \cdot (\tau_s + \tau_8 + \tau_{8e})}{(\tau_m + \tau_e + \tau_s) + (\tau_s + \tau_8 + \tau_{8e})} \quad (15)$$

Thus rewriting equation (13):

$$n_e = (1 + \frac{\tau_e}{\tau_r} + \frac{\frac{(\tau_m + \tau_e + \tau_i) \cdot (\tau_i + \tau_8 + \tau_{8e})}{(\tau_m + \tau_e + \tau_i) + (\tau_i + \tau_8 + \tau_{8e})}}{\tau_d} + \frac{\frac{(\tau_m + \tau_e + \tau_s) \cdot (\tau_s + \tau_8 + \tau_{8e})}{(\tau_m + \tau_e + \tau_s) + (\tau_s + \tau_8 + \tau_{8e})}}{\tau_n})^{-1} \quad (16)$$

This gives the expression for  $n_e$  in function of the different transition periods.

We could simplify this term: because the newly introduced state  $n_8$  is only getting the overhand for higher laser powers, we can assume that  $\tau_8 \gg \tau_e, \tau_i, \tau_{8e}, \tau_s$ . Therefore by neglecting the corresponding terms and recasting it in function of the transition rates, we get for the population of NV centers in the excited state:

$$n_e = \frac{1}{1 + \frac{k'_r}{k'_e} + \frac{k'_d}{k'_m + k'_8} + \frac{k'_n}{k'_m + k'_8}} \quad (17)$$

From the five level state, we already know that  $k'_e$  and  $k'_d$  are depending on laser power, for the six level system to be useful,  $k'_8$  must also be depending on the laser power. Thus from (5), we get:

- $k_e$ :  $k'_e(P) = k_e P$
- $k_d$ :  $k'_d(P) = k_d P$
- $k_8$ :  $k'_8(P) = k_8 P$

Letting the other k's constant and filling above functions and keeping in mind the proportionality constant  $a$ , we get for the fit:

$$g(P) = \frac{a}{1 + \frac{k_r}{k_e P} + \frac{k_d P}{k_m + k_8 P} + \frac{k_n}{k_m + k_8 P}} \quad (18)$$

We confirm:  $P \rightarrow \infty, g(P) \rightarrow \frac{a}{1 + \frac{k_d}{k_8}}$ , giving the asymptotic we see in figure 8.

In this thesis, a big part of our experiments will be about measuring the saturation curve of the excitation wavelengths in the range  $535\text{nm} - 570\text{nm}$ . We will try to find the transition time for this hypothetical state for the different wavelength by using the function  $g(P)$  as fit, which should give back the values of the k's.

### 3.5 Density of states

If there is no source of energy to excite the NV center, the transition period,  $\tau_e$  from ground to excited state, will be infinity. The laser will serve as a energy source, changing  $\tau_e$ , concluding this transition period is depending on the laser power. This insight results in the fact that other transitions, and the corresponding populations, will be also changing through time. These populations will be constant when we'd consider a time scale big enough, but when we'd shorten the time range sufficiently enough, there are still many transitions going on.  $n_e$  is calculated by comparing the time, T, a population of NV centers in the excited state with the time that the other populations of NV centers are in other states, giving the method of density of states:

$$n_e = \frac{T}{T + \sum_i N_j t_j} \quad (19)$$

$N_j$  represents the number of events of a certain type of event(this could be radiation, ionization, deionization, ...) during the time T, and  $t_j$  refers to the time between the end of the type of event and being back in the excited state. Note that this fraction already tells us that the more states, and so the number of possible transitions, other than the excited state there are, the less populated  $n_e$  will be.

We can simplify equation (19) by revisiting the physical meaning of  $\tau$ : this meant the transition period, so every  $\tau$  time, the corresponding transition will happen, therefore we can say that  $N_j = \frac{T}{\tau_j}$ , giving for (19):

$$n_e = \frac{1}{1 + \sum_i \frac{\tau_j}{\frac{T}{N_j}}} = \frac{1}{1 + \sum_i \frac{\tau_j}{\tau_j}} = (1 + \sum_i \frac{\tau_j}{\tau_j})^{-1} \quad (20)$$

With this description, the derivation of (7) becomes clear. As an example, let us calculate the term corresponding to the deionization  $n_e \rightarrow n_0$ . The transition period is given by  $\tau_d$  and the time to get back to the excited state is given by the sum of all inner-transitions  $n_0 \rightarrow n_m \rightarrow n_g \rightarrow n_e$ , giving  $t = \sum_i \tau_i = \tau_i + \tau_m + \tau_e$ . So in total, we get the expression:

$$\frac{t}{\tau_d} = \frac{\tau_i + \tau_m + \tau_e}{\tau_d}$$

This is the third term in (7)

## 4 Experimental setup

To measure the photoluminescence, following 'confocal' setup was used:

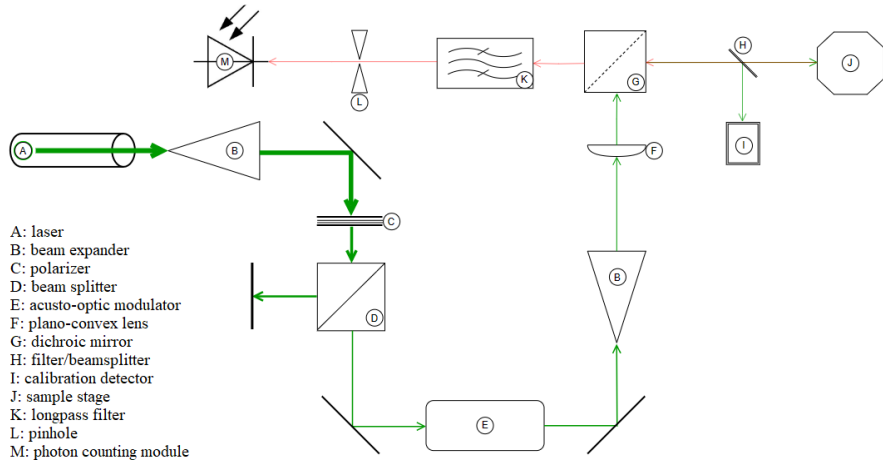


Figure 9: Experimental setup for measuring point defects in diamond.

Firstly, the SOLSTIS EMM laser, manufactured by Msquared, sends a light signal with a wavelength varying between  $535\text{nm}$  and  $570\text{nm}$ . To reduce the power of the laser signal, there has been introduced several beam expanders and a PBS201 beam splitter, both from Thorlabs. As the names suggests, the beam expander diverges the collimated beam from the laser, and only lets through a part of it, reducing the light intensity and therefore the power associated with it. The beam splitter further decreases the intensity. This gives the possibility to use powers ranging from  $0.5\text{mW}$  all the way up to  $80\text{mW}$ .

These devices decrease the power by a fixed value, causing practical issues. To resolve this problem, there was also introduced the polarizer. The polarizer surpasses light with a certain polarization, and since the laser beam is highly polarized, it gives rise to the possibility of fast and effectively changing the intensity. This is done by manually turning a wheel of the polarizer to change the preferred polarization. The fact that . In our experiments, there was also a acousto-optico modulator (AOM) present in the setup to create light pulses, but this wasn't used by our main setup.

The AOM was used to create the pulsed laser in measuring the Rabi oscillations at another setup located in the same room which was identical to ours but with a magnetic source above the sample stage. As stated in the theory section, due to the presence of external magnetic field, the degeneracy of the  $m_s = \pm 1$  state is being lifted. As a consequence, we would get a sum of two Rabi oscillations so that the magnetic field splits the degenerate states, detecting one individual sinusoidal signal and not two.

Once the signal passes through the last beam expander, it is being led through a plano-convex lens to be collimated. It is important for the dichroic mirror to be highly effective. This mirror transfers all the light with a wavelength higher than  $580\text{nm}$  and reflects light beams lower than that. This means that the light coming from the laser is being reflected and sent to the filter. This filter has the purpose to send a fraction of the light to the PDA10A2 calibration detector of Thorlabs to accurately choose the excitation wavelength.

The light that goes through the filter is being send to a mirror which vertically reflects the light to the P-5613CD piezoelectric motor from PI controllign the sample stage. At this stage, the beam is being converged onto a point on the sample and it will excite the molecules inside that subarea of the diamond lattice. The NV center photoluminescence

of the NV-center is in the range of red light and beyond(see Theory section). Our setting is designed to measure between the wavelengths 580nm and 1000 nm, which means that the infrared transition of the NV center at 1142 nm will not be detected. The dichroic mirror which gives the lower limit is not perfect and there can still pass some light with a wavelength below the 580 nm, to reduce this inaccuracy, there has also been added a longpass filter to filter as much as possible the remains of initial laser light.

At last, this image of the point the laser is focusing on, is being led through a pinhole. This pinhole serves to block the out-of-focus light in the formation of the image[13]. Once the light passed through the pinhole, the image of a single point on a inner surface of the diamond is collected by the SPCM-AQRH-14 photon counting module of Excelitas. By moving the piezoelectric motor in the plane, a whole image of the inner-surface can be constituted, whereafter it gets visualized by 'Kernel'(see section 4.2.1) and further analysed.

#### 4.1 NV-center sample

The sample stage for the NV-center could be schematically described as: The 6221 DC

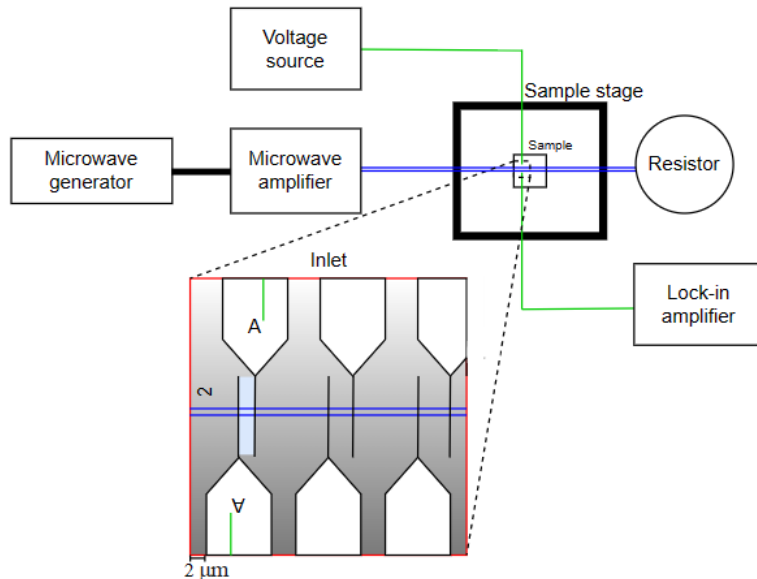


Figure 10: Experimental setup for measuring point defects in diamond. Inlet gives the nanoscaled structure of the used sample.

and AC current source was used as voltage source to create a potential difference in the sample, forming a photocurrent, which will be registered by the MFLI lock-in amplifier of Zurich Instruments.

To get ODMR, there is need of a microwave signal generator. The microwave signal was created by the SHFSG of Zurich Instruments, but the amplitude of this signal is too weak. Therefore it is amplified by the ZHL-5W-202-S+ high power microwave amplifier of Mini-Circuits Instruments. The amplified signal is send through wires which radiate off the microwaves on the sample. To have a closed circuit, this wire is brought back to the amplifier through a resistor of  $50 \Omega$ . The resistor is placed so that the two signals, going from and to the amplifier, would constructively interfere.

The NV-sample is being sectioned into different sections; going from 1A to 3F. As seen in the inlet, the wires from the voltage applier to the lock-in amplifier are connected at the electrodes of section 2A. The wires for ODMR are also present in this section. Therefore is

was concluded that the blue zone(width:  $2\mu\text{m}$ ) would be the best to search for the effects associated with the NV-centers.

## 4.2 Main procedure to find a NV-center

Before there can be done any measurements on the NV-center, the center must firstly be found in the millions of other defects in the sample. This is done by following the 'standard' plan described below.

### 4.2.1 Labview program: the 'Kernel'

Due to the fact that the experiments are in order of micrometers, there is use of a Labview program, called the **Kernel**. This Labview program sends commands to the setup, while receiving data from the different devices in the setting, such as the photon counting module.

### 4.2.2 Rough alignment of the sample

Before any fine alignment, the preferred blue zone(see inlet 10) must first be located. This is done by placing a paper in front of the long pass filter and manually locate the position of section 2A. Once this is done, there can be made maps of this area by the detector, which is then send to the Kernel.

### 4.2.3 Mapping of inner-diamond surfaces using the confocal setup

As earlier stated, due to the confocal setup the laser beam converges onto a point on the sample and excites the molecules in the diamond in that particular area. These emissions will go through the dichroic mirror and pass the pinhole to give an image of that small region. Together with the movement of the piezoelectric motor, a full image of an inner-surface of the diamond can be fetched together, resulting in a image/map of this inner surface of the diamond(see 11). This map is based on the intensity of the photoluminescence: spots which give a higher photoluminescence, are represented by brighter spots on the map. These bright spots give a good guidance to find the (relatively bright) NV-centers.

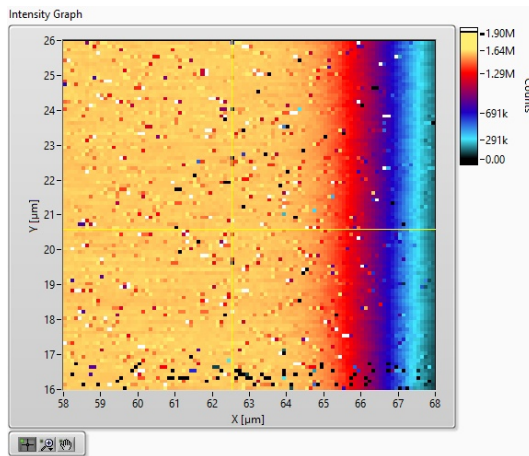


Figure 11: Example of the mapping of an inner surface

### 4.2.4 Finding the brightest spot

The mapping is only done in two dimensions: (x,y) coordinates, while the diamond is three dimensional: (x,y,z). To solve this problem, we hovered over the sample with the mouse

cursor to find the brightest spot, whereafter we lowered or highered the sample stage with the piezoelectric motor.

#### 4.2.5 Using ODMR to find a NV-center

Due to the rough alignment, the blue zone where the NV's will be searched is already on the new map. But to find a NV-center, only looking at the maximal photoluminescence isn't enough. To ensure ourselves, there are two ways:

1. Using ODMR: measuring the EPR-spectrum and check if there is a dip around 2.87GHz.
2. Adding the Newton 970 EMCCD spectrometer from Andor at the setup(see 12) and control if the shape of the emission spectrum is reminiscent of that given in the theory section.

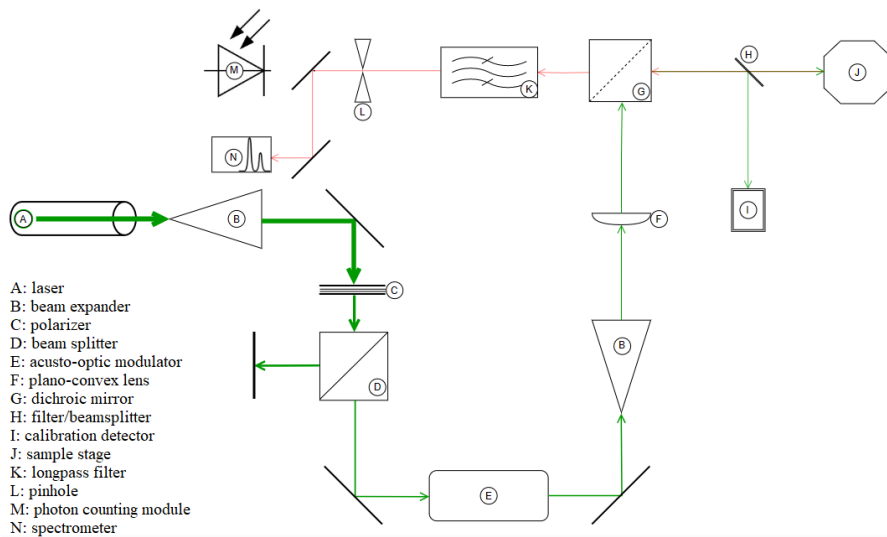


Figure 12: Experimental setup with spectrometer.

In the following sections, the results will be discussed.

## 5 Experimental Results and Discussion

In this section an overview of our experimental results follows. Since many experiments have been performed, we'll be focusing on the most significant ones:

- Finding and confirming single point defects in diamonds using ODMR and spectrum analysis.
- Experiments to verify PL dependence on applied voltage, at different laser powers. Discussed are voltage sweeps from -20 to 20 volts at different laser powers, and Rabi-oscillation measurements
- Saturation curve measurements, for the experimental validation of the hypothesized sixth state in NV-centers, and our approach to retrieve the parameter for  $k_8$ .

Other experiments and their results can be found in the appendix, and are linked subsequently in the public GitHub repository. All experiments have been performed on sample #213, which can also be seen on figure 13.

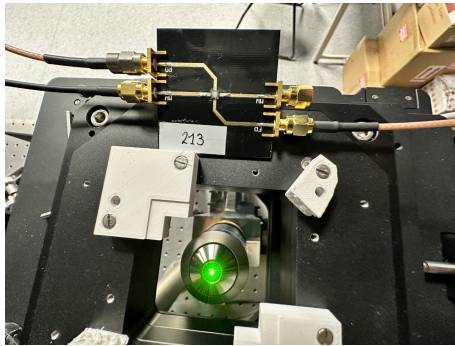


Figure 13: Sample #213 next to the piezo-electric stage. Attached are potential and microwave cables to electrodes within the sample

### 5.1 Finding and verifying NV-centers

To find an single point defects (NV-centers) on a lab-grown sample, the crystal grower specifies on which electrodes the outer connections are attached, such that relevant physical signals can be provided to the diamond. On sample #213 the active electrodes are labeled with *A2*, which indicate the *A*th row in the 2nd column on the sample. A microscope image of these electrodes can be seen on figure 14.

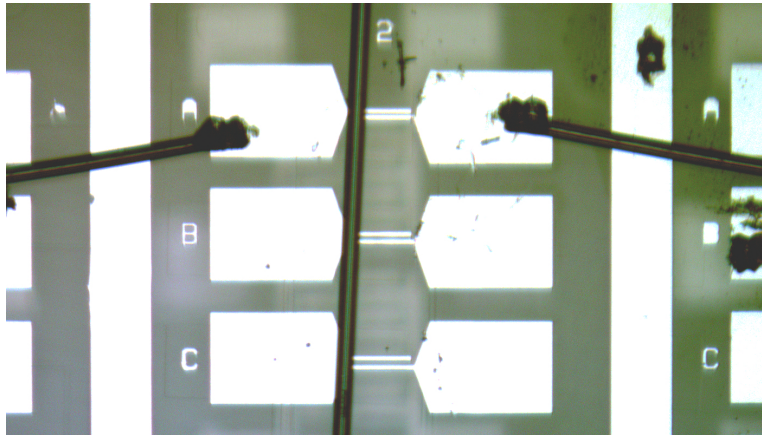


Figure 14: Sample #213 A2 electrode locations.

Alignment of the objective and stage on this tiny region (*A2*) as discussed in the previous section requires a coarse/rough alignment, using unfocused optics to produce an image on a piece of paper. The coarse-alignment is done using screws which are attached to the stage. Once coarse-aligned is completed, a region scan (map) is obtained using the *kernel software* in LabView. It's important to note that mapping the diamond region of the sample is done using a low laser power (2mW max). Obtaining a map is a process which is time intensive because the piezo-electric stage is required to make 10k ( $100 \cdot 100$ ) individual measurements (photoluminescence) across a designated region. This process is sped up by using a lower integration time (30 ms).

A typical first overview map of a region can be seen on figure 15, where the *A2* electrodes are seen as two bright pillars. We are interested in studying NV-centers between electrodes, which requires a finer scan. Figure 15 shows also two finer maps of the in-between electrode region, which is respectively  $30\mu m \cdot 30\mu m$  and  $10\mu m \cdot 10\mu m$  in size. Using this map, the width between the two bright pillars can be measured, which coincides with the sample-supplier's specifications of *A2* electrode's width:  $\pm 2\mu m$ .

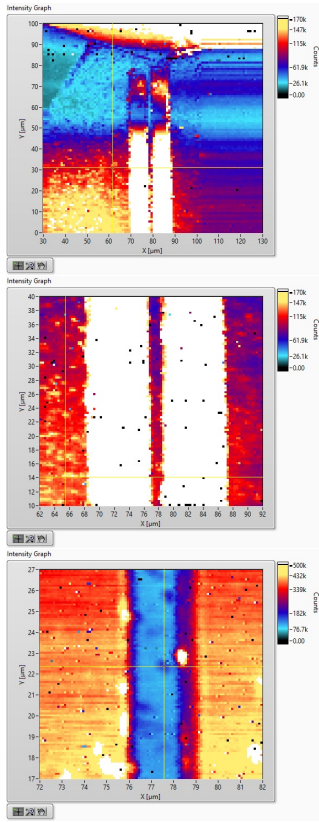


Figure 15: Sample # 213 on progressively zoomed levels. Color map shows photoluminescence (counts / seconds).

It merits to mention, that obtaining a good-looking map of a defected diamond region is an iterative process, where positioning, alignment, and z-depth are progressively tweaked, to arrive at a working map.

Once the map is sufficiently fine-tuned, NV-center will show up as slightly more luminescent than the surrounding background. A cursor on last figure of 15 can be seen centered on a single-point defect. The next step involves finding high-PL regions using the *kernel's* cursor, then verifying the various NV-center properties using ODMR and spectrometer analysis.

### 5.1.1 ODMR Spectrum Analysis

The hallmark way to verify the presence of an NV-center, is to apply a microwave sweep in a range from 2800 MHz to 2900 MHz, then looking for a PL dip at a specific frequency. Each NV-center, before studying its properties at different physical environmental changes, has been subjected to this ODMR spectrum analysis, to verify that the optical bench is well focused and targeting an actual NV-center. One out of many measured ODMR spectrums can be seen on figure 16. The resonance frequency is measured at 2871 MHz, and this frequency will be used later in experiments, to consider environmental changes due to applied potential.

Seeing a dip in photoluminescence, like on figure 16, is enough evidence to conclude that the optical bench is indeed focused on an NV-center. In case of doubt, one can another layer of verification to this ODMR-spectrum analysis: a physicist can apply a magnetic field to the sample, which will split up the population of the triplet states, thus causing a Zeeman-effect, which will split the ODMR-dip into two dips, a specific distance away from the original resonance frequency. We've performed this type of verification only a

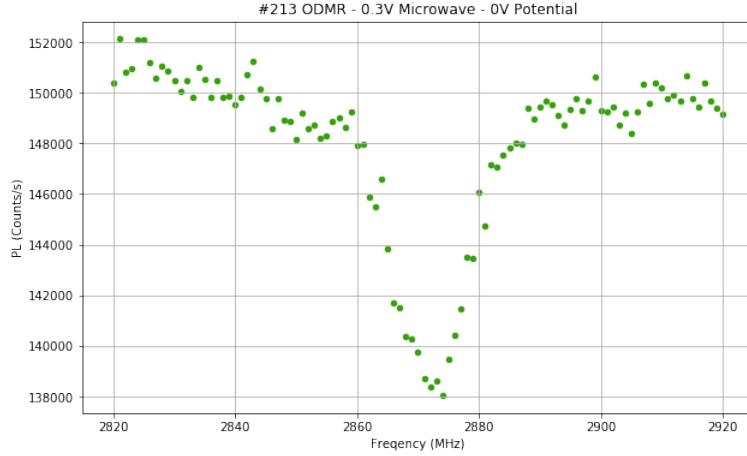


Figure 16: ODMR at 0.3V microwave potential, and 0V applied across the electrodes. The resonance frequency is measured at 2871 MHz.

few times when our measurements seemed to be way off, and what came out was that a few lenses weren't well focused on the objective. For our purposes, however, performing ODMR spectrum analysis without a magnetic field was more than adequate.

### 5.1.2 Frequency Spectrum Analysis

Another way to verify the presence of an NV-center is by obtaining the frequency emission spectrum. Typical of an NV-center's spectrum is a peak at 638nm-642nm which represents the zero phonon line (ZPL), with a *hill* at higher wavelengths to the right of ZPL which goes well into the IR region, which is representative of the so called phonon-wind. On figure 17 one can observe these indicators. This data was obtained by subtracting a background spectrum from an NV-center spectrum, which is a time intensive process, and hence why spectrum verification wasn't performed for each NV-center encountered, but mentioned for completeness.

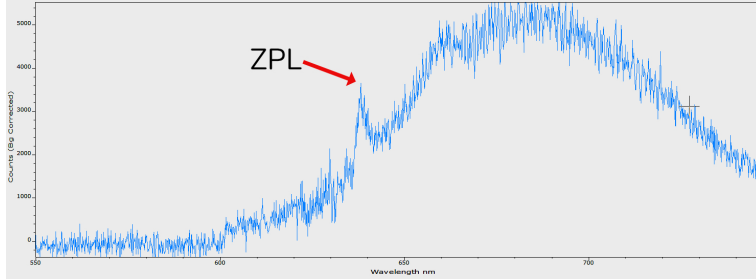


Figure 17: Frequency Spectrum of an NV-centered. ZPL is clearly seen, followed by phonon wind

## 5.2 PL / PC dependence on applied voltage

In section 5.1 the required steps for the finding and verification of a single-point defect are discussed. Now that an NV-center is located and verified inside the sample, we'll focus this section on measurements which relate to the suspected PL dependence on applied voltage.

The main idea for the experiments performed in this section is that researchers at the Photonics Department at IMO IMEC have been performing photocurrent (PC) research of

NV centers with the assumption that different applied potentials on the sample's electrodes does not influence the crystal's environment, and thus should not influence PC nor PL at different voltages. It bares to note that most of this research has been done using lower laser power, and has been communicated to us via our promoter and assistants.

### 5.2.1 Voltage Sweeps

We'll be discussing a series of performed measurements, to verify this claim, or perhaps challenges made assumptions. To this end, we apply a voltage sweep to the sample's electrodes, from -20V to 20V, in one direction. The laser's wavelength is chosen at 535nm (green) and set at 2.4mW unless otherwise specified. An NV-center is chosen which is near the electrodes (less than  $\pm 1$  nm) as to clearly measure any voltage dependence.

Initially, PL measurements are obtained at the ODMR resonance frequency (2871 MHz) as obtained in section 5.1.1, at a non-resonant frequency (2800 MHz) and with microwave turned off. For elegance, the experiments are performed at two different microwave amplitudes: 0.25V and 0.4V. Obtained results are smoothed using a Savitzky–Golay filter allowing us to inspect the contrast in greater respect, and the results can be seen in figure 18.

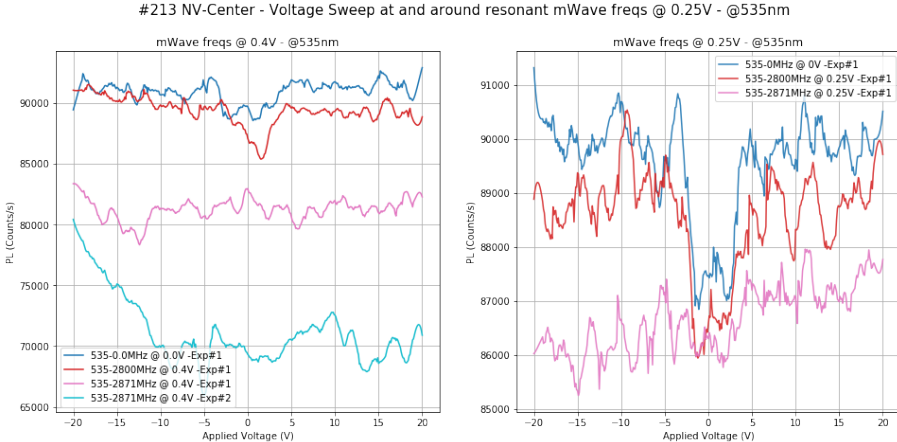


Figure 18: PL at varying voltage sweeps, at different microwave frequencies and amplitudes.

It's clear from measurements that the overall PL is reduced across the voltage sweeps at the resonance frequency (2871 MHz). This is in alignment with ODMR spectrum measurements. PL counts seem to drop significantly between -2.5 and 2.5V when *microwave is at non-resonant frequencies, and when the microwave is turned off*. Where a contrast is to be witnessed, it seems to be larger when the microwave is on (at non-resonant frequencies), and less when the microwave is not enabled. The overall PL drop contrast is observed to be of the same order ( $\pm 3$ k counts/s without microwave,  $\pm 4$ k counts/s with microwave turned on) when comparing different microwave amplitudes.

We've included a slightly weird result on figure 18, in particular experiment 2 at 0.4V microwave amplitude at 2871MHz. Here we can see a steady drop-off of PL between -20V and -5V. An educated guess points in the direction of sample drifting. In fact, all measurements conducted in this report, with microwave turned on, that the sample was drifting. Every few minutes, a single point defect had to be relocated, before conducting more experiments.

To obtain a better picture to the actual difference between 2800MHz and 2871MHz microwave measurements, and no microwave and 2871MHz measurements, we've subtracted the PL counts, and smoothed out the result using a Savitzky–Golay filter. The results can

be seen on figure 19.

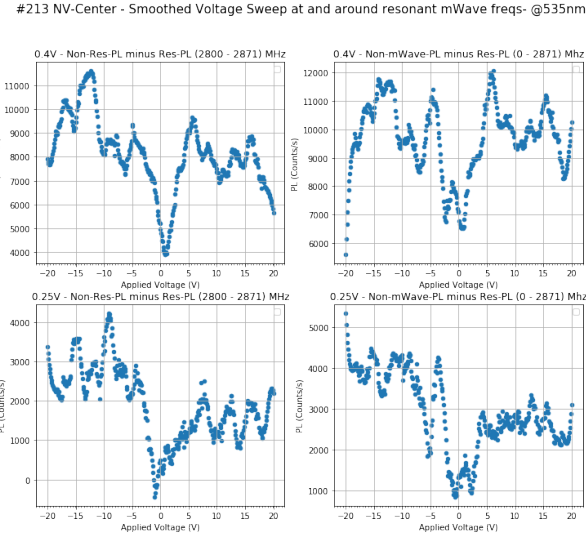


Figure 19: Subtracted PL counts from figure 18 at varying voltages and microwave amplitudes

From our measurements we can conclude that at the resonance microwave frequency, the PL decrease due to voltage changes is effectively eliminated. Further, we're observing a quite weird but interesting periodicity and sawtooth-like pattern emerging in these (difference) measurements. We've highlighted these in figure 28, 29, and 30 in the appendix. We're not sure if these patterns are significant, or if they might be an artefact of the applied Savitzky–Golay filter to smooth out the data. Results from these voltage sweeps are interesting and cause us to ask the following questions for future research:

- Why is PL affected by changing voltages, particularly at non-resonant frequencies?
- Is there a certain periodicity or periodic spin state manipulation occurring within the inner 'circuit' of an NV-center?
- How would these measurements look like with a pulsed laser?

We'll shortly discuss if we're noticing a significant photocurrent change with and without microwave applied the sample. Measurement results can be seen in figure 20, in which outliers have been deleted. We're noticing a significant deviation at voltages higher than  $|15|V$ , for which we don't have an immediate explanation. The slight change in PC starting from 0 and finishing at 5 are indicative of noise or sample drifting.

Discussed now are voltage sweep experiments related to different laser powers, in particular at 2.43mW and 31.5mW. NV centers, used in quantum sensing research, are often studied at a laser power with no more than 4mW (Cube reference), since at laser powers higher than that ODMR spectrum are observed to start to fall apart and making it highly unreliable, we've observed this in our own experiments as well. It's not worth showing the results, as it would be like showing a noisy signal. We're mentioning this, because the following experiments are conducted with no microwave enabled. Voltage sweeps for PC and PL can be seen on respectively figure 21 and 22.

When analysing the PC data, we're observing a similar trend to our previous PC measurements - a sudden increase from 0-1V, then flattening again, only to exponentially increase at the higher voltage regions. Both low and high laser power are showing similar patterns, for both NV-centers (which are at different locations).

When analysing the PL spectrum, location 1 shows a very peculiar pattern: at low laser

Sample #213 - PC - Voltage Sweep - At resonant 2871MHz microwave, and without applied microwave

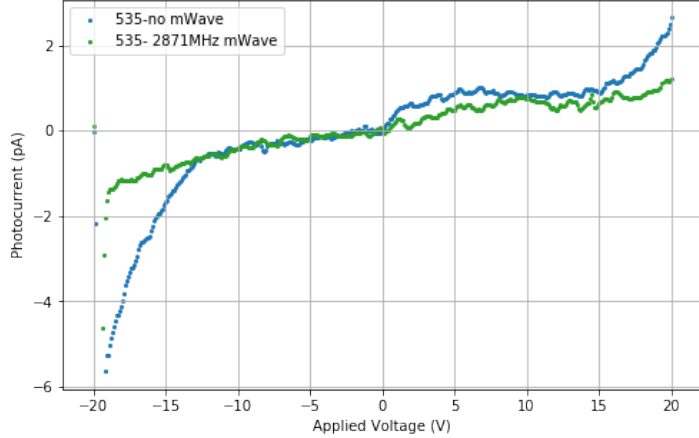


Figure 20: PC (pA) for varying voltages at 2871MHz and no microwave

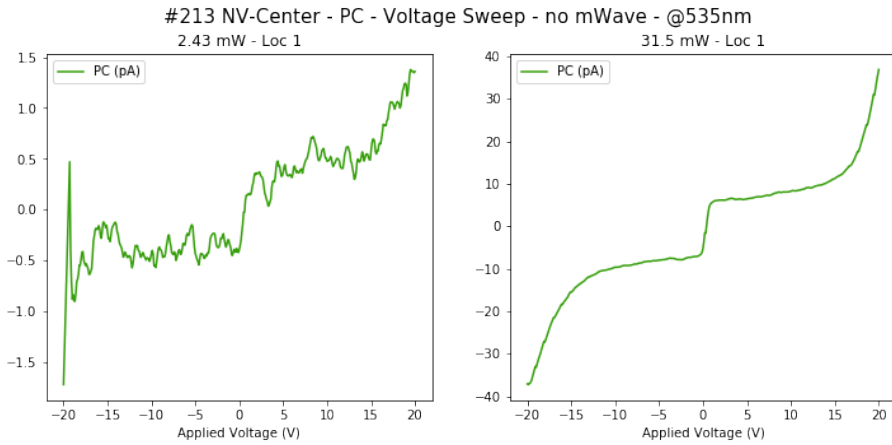


Figure 21: PC voltage sweeps at low and higher laser power

power there's a dip in PL between the previously seen -2.5V and 2.5V range. **At a high laser power, the dip region is measured as an increase in PL!** We're not quite sure what to think of it, but to measure many voltage sweeps across a wide variety of laser powers, to observe any linearity in this change, and further, if there's a laser power where PL doesn't change when varying voltages. For completeness we added the rather noisy data for location 2, which is most likely due to drifting of the sample during measurement. We'll call the laser power at which no PL difference is measured when varying the applied voltage the **point of interest**.

### 5.2.2 Point of Interest

We call the the laser power at which no PL difference is measured, when applying a voltage sweep, the **point of interest**. To obtain the point of interest, we're performing voltage sweeps at increasing laser powers, from 2.4mW to 24mW, in steps of 5mW. To make the data significant, we're performing a total of 10 voltage sweeps for each laser power, then averaging over the results. We've also opted to increase the integration time across the voltage sweeps, to increase accuracy of the measurements. The absolute PL counts of these measurements can be seen in figure 31 in the appendix. For our purpose, we're interested in the relative contrast in PL change when varying voltage, at different laser powers. The results are smoothed using a Savitzky-Golay filter to make the data easier

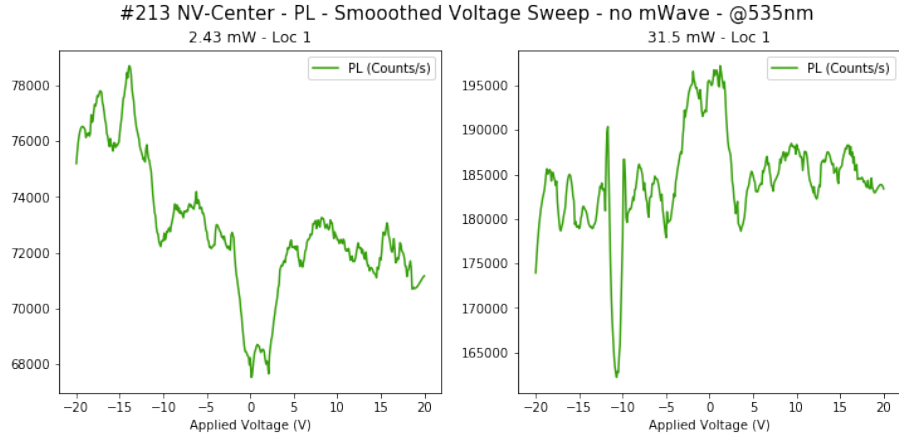


Figure 22: PL voltage sweeps at low and higher laser power

for interpretation. The results can be seen on image 23.

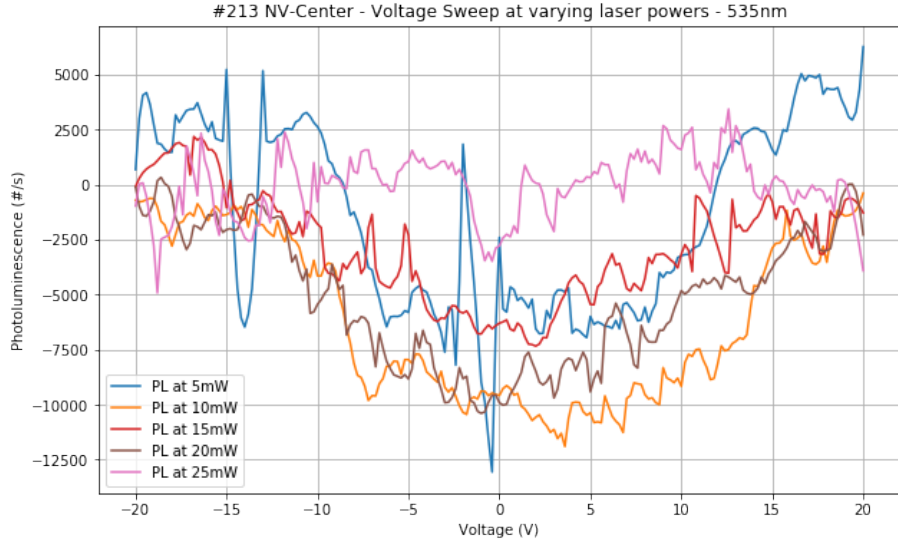


Figure 23: Point of Interest - relative PL during a voltage sweep at different laser powers

Point of interest measurements are now being discussed. We notice first of all, that there's no increase in PL at high laser power, noting however that we didn't perform measurements at laser powers at 30mW and up, where we previously noticed this increase in PL occurring. There's a tendency of the PL to tend to zero as laser power goes higher, at 25mW we see that the PL remains relatively stable.

Further analysis of the curves reveals qualities which we don't know how to explain, and require further investigation and research:

- Why is the relative PL change at 10mW and 20mW laser power coinciding so well?
- Why is there a sudden shift to zero PL change from 20mW to 25mW?
- How would the measurements look like at laser powers 30mW and up?
- How would the measurements look like with a pulsed laser?

To shine light on some of these questions, we opted to measure several saturation curves at different applied voltages (-10, 0V, 10V), with the aim to find a laser power at which

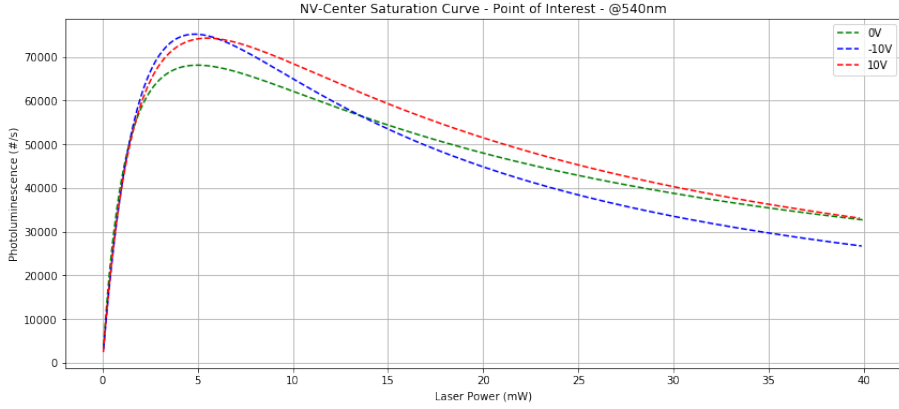


Figure 24: Saturation curve to obtain the hypothetical Point of Interest

the saturation curves (at -10V, 0V and 10V) would cross, and thus revealing the actual point of interest. We opted to increase the laser wavelength to 540nm, perform 6 saturation curve measurements at each voltage, then fitting the curve and analysing the results.

For completeness, we mentioned the required steps too obtain an appropriate saturation curve for a given laser power, given our experimental setup:

1. **Obtain a linear regression to map Volt-to-mW.** This is required because our setup uses voltage to capture laser power in our data, and we're interested in a PL-mW curve. Measure V and MW at 2mW, then at almost max power ( $\pm 40\text{mW}$ ), after which, fit the curves.
2. **At 2mW, find an appropriate NV center**
3. Go to minimal laser power by turning the polarizer to zero
4. Start recording PL-mW data, and gently rotate the polarizer to put more power to the NV center
5. Stop measuring data when reached max power.
6. **Now go to a background location** (where no NV center is located), and repeated the previous 4 steps. This is to obtain the background PL, allowing us to subtract the background PL from the NV-caused PL, and thus obtaining an indicative saturation curve.

It's important to note that our setup changed a few times during our measurements during the months, resulting in an ever increased laser power output of the setup, a change in optics setup and alignment, creating extra challenges to obtain consistent data.

The resulting 18 different measurements have been captured and fitted using our modeled equation 18. The resulting saturation curves for -10V, 0V and +10V can be seen in figure 24. When analysing this data, we're looking for a cross-section between the 0V curve and the -10V and 10V curve. According to the saturation curves, this would coincide with 13mW and 40mW. This is not in alignment with our previous point of interest measurements.

The reasons for this might be many-fold: capturing saturation curves on our setup required the **manual turning of the polarizer during measurement**. Since our measurements concern a micrometer scale, it's safe to say that it would be impossible for us to turn the polarizer by hand without perturbing the sample and stage. In fact, we've observed that claps and slight touches of the optical table create vast streams of noise in captured

data. Thus we recommend installing a piezo-controlled motor for rotating the polarizer systematically and mechanically.

Further reasons for discrepancies in measurements could be due changing circumstances of the crystal lattice, when shining a high laser powered on the NV-center, which might be contributing to non-linear effects. For future research it's suggested to introduce a cooling system to cool the sample itself, down to a few decimal kelvin, to keep the inner lattice of the crystal as stable and consistent as possible during experiments with high laser power bombardment.

The above reasons, although valid and reasonable, don't seem to be touching the core attributable issue to our perceived discrepancies, which begs the question if something else might actually be happening. To spoil the conclusion of the upcoming section, and this realization came pretty late in our whole experimental journey: initialization issues are probably at play, which gives result to a vast array of quite inconsistent results, more on this in section 5.2.3.

### 5.2.3 Revealing ODMR and Rabi Oscillations at different voltages

The bulk of the experiments mentioned thus far are concerned with detecting changes of the environment and thus properties of the NV centers, when affected by different applied voltages on the electrodes. In this section, we'll discuss experiments done to analyse the true and trusted ODMR spectrum analysis and how it is affected when applying a varying voltage potential.

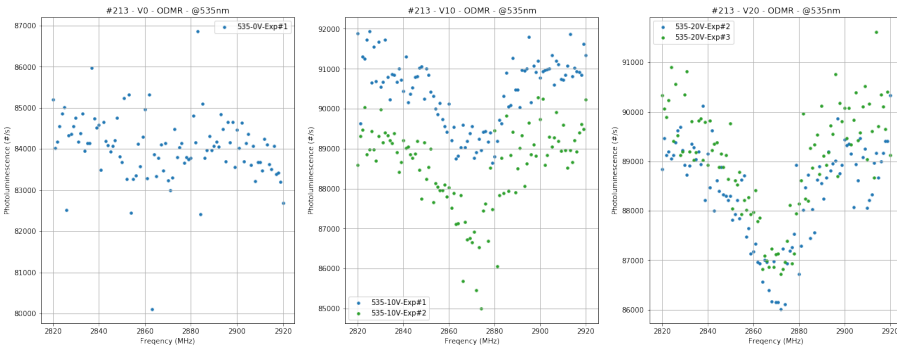


Figure 25: ODMR at different applied voltages. Notice how the contrast at 0V is absent, but it is present at 10V and 20V.

Similar to previous experiments, we turn the laser down to 2.5mW to ensure a correct ODMR measurements, and we tune the laser to 535nm. An NV center is chosen less than  $1\mu m$  away from the electrodes. We conduct ODMR spectrum analysis at 0V, 10V and 20V. The results can be seen in figure 25.

Immediately noticeable is the data obtained at 0V, where we notice an **absence** of a PL dip at the typical resonance frequency of 2871 MHz. How can this be? At 10V and 20V we're consistently able to produce a well defined ODMR spectrum with a clearly visible resonance frequency, yet each time the applied voltage is *returned back to 0V*, the ODMR spectrum is severely lacking in its indicative properties of the presence of an NV center. Even more confusingly, our first ODMR spectrum measurements as presented in this paper were conducted on 0V, which didn't show these deviations from sanity. Perhaps our setup was deeply anomalous in some sinister yet invisible way?

To better understand the confrontation with these measurements, our department colleagues were gracious enough to lend us a different setup for a few days, which is equipped

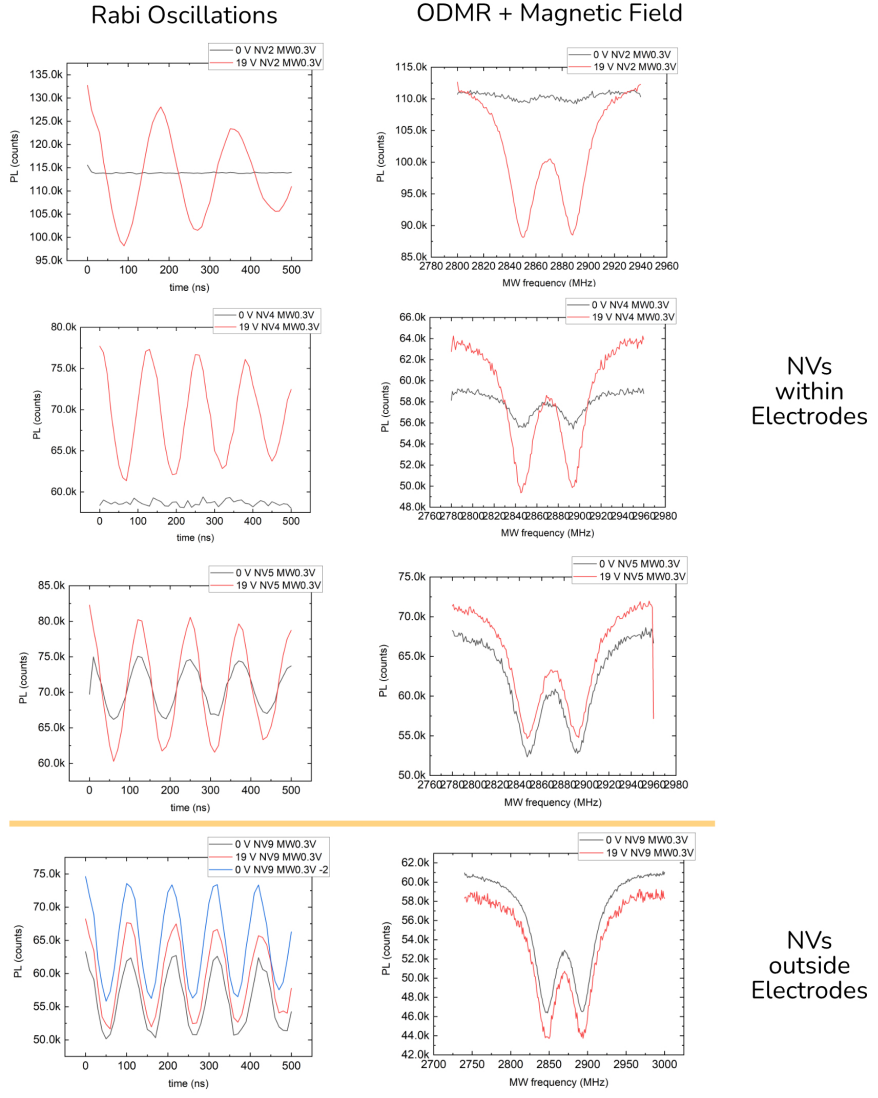


Figure 26: Point of Interest - relative PL during a voltage sweep at different laser powers

to perform Rabi Oscillations measurements, and ODMR spectrum analysis with an extra applied magnetic field.

Upon installing sample #213 on the new setup, we performed a series of Rabi Oscillation and ODMR with magnetic field measurements on different NV centers located between the electrodes, and a few outside of our electrodes. Each measurement was done at 0V and 19V. The resulting measurements can be seen in figure 26, and are quite revealing.

**Between the electrodes**, at 19V, we observe nice sine-wave-like Rabi Oscillations, and a cleanly split ODMR spectrums (the splitting of resonance frequency into two is due to an applied magnetic field). At 0V, we observe that the same NV-centers produce very inconsistent or absent Rabi Oscillations and ODMR spectrums. We notice this effect especially when cycling between 0V and 19V: 19V gives nice and expected results, whereas 0V gives unexpected and non-indicative results. To put emphasis on the inconsistent nature of this observation, take note on our results on figure 26 for NV5: at 0V the Rabi Oscillation has a completely different amplitude than what it is at 19V, whereas the subsequent ODMR spectrum measurements show a very similar contrast for both 0V and 19V.

When conducting the same experiments on NV centers **outside of the electrodes**, we observe that both 0V and 19V Rabi Oscillations and ODMR Spectrums give the same contrasts, no matter how many times we've cycled between 0V and 19V.

Discussion with our assistants, colleagues and promotor lead to the conclusion that we're witnessing initialization errors: when cycling from 19V to 0V, the ground state of the NV-center is not populated fully at state  $|0\rangle$ , but is most likely dispersed across the different states which characterize an NV-center, and thus causing an inconsistent PL-process throughout the modeled level states of an NV-center. The following research questions arise for future research:

- What is the theoretical cause for bad initialization after varying voltage, and especially from a 'potentialized' (meaning non-zero voltage) state to 0V?
- How can one initialize an NV center correctly, after application of potential, and then removing it?
- Is the same behavior expected with a pulsed laser? is the initialization issue presented with a pulsed laser?

As a final conclusion to this section, we can safely say that the many discrepancies and seeming anomalies between expectation and measurement were due to initialization issues, which were only revealed after many performed measurements. By addressing this issue, and by conducting a fundamental analysis of initialization dynamics of NV-centers, better and cleaner results can be made, to further understand the potential changing properties of NV-centers when subjected to varying potential conditions.

### 5.3 Saturation curves, $k_8$ and asymptotic behavior

In the theory section of this report, the existence of a sixth state is discussed as reported in literature [9] and at Photonics Department at IMO-IMOMEC [11] [10]. To verify this sixth state, saturation curves at different wavelengths are obtained. The saturation curves are subsequently fitted using equation (13) to obtain an adequate value for  $k_8$ , which is the rate at which the spin population at the metastable state migrates to  $k_8$ , which in case this state exists, should show up as non-zero asymptotic behavior in non-infrared PL at high laser power. We remind the reader that our setup measures PL with a filter cutoff at 1000 nm, meaning that IR PL is neatly filtered out. If the sixth state does not exist, we should be seeing PL drop off to zero at high laser power, as our investigated spectrum range gets effectively saturated.

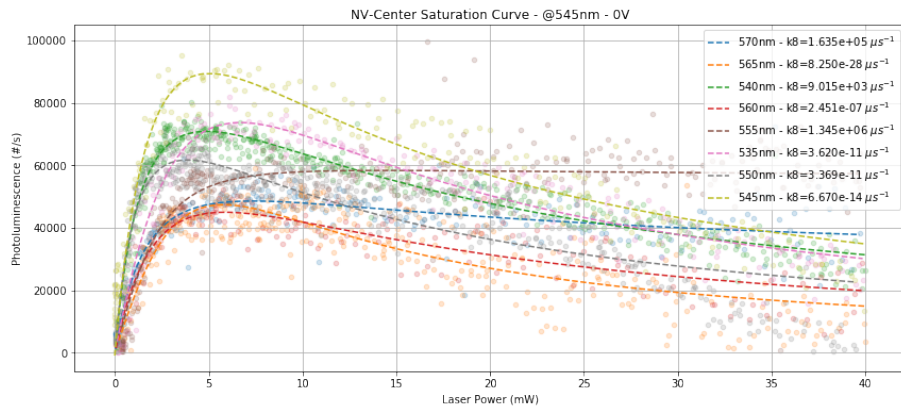


Figure 27: Saturation curves at different wavelength, fitted assuming the existence of a 6th state

The procedure to obtain saturation curves has been outlined in section 5.2.2. A total of 105 saturation measurements have been conducted at from low to high laser power, of which 73 concern NV center PL measurement, while the remaining 32 concern background measurement to procure an adequate background PL subtraction to obtain the desired saturation curves. Wavelengths starting from 535nm till 570nm have been measured, in increments of 5nm.

For the same reasons as outline in section 5.2.2, we were required to reject many measurements due to unclean data. That's because our setup suffers from a fatal flaw: manually turning a polarizer to obtain a saturation curve, which caused visible perturbations and plainly weird saturation curves. A total of 32 out of 73 measurements had to be discarded due to weird perturbations and wrong measurements.

The results of our measurements, together with fits for each wavelength can be seen in figure 27. Measurements for each wavelength are bundled together into ensemble datasets, which are then fitted. Figure 27 also shows the fitted value for  $k_8$ , which is almost-zero (or irrelevant) for saturation curves which tend to zero. In fact, all saturation curves show a clear tendency to reach zero, except for wavelengths 555nm and 570nm. Wavelength 540nm shows a non-zero  $k_8$  of  $1.6\mu\text{s}^{-1}$ . Though we've performed measurements from 0mW to 80mW, we've cut off our measurements at 40mW, since beyond that we noticed that the data shows increasing instability at higher wavelengths (555nm and up). We include measurements up to 80mW in the appendix.

The fitting of these curves have been a journey on its own, since equation 18 has 5 degrees of freedom, which makes the searching space for an adequate fit exceedingly hard, especially if fitted value for  $k_8$  ought to hold a physical meaning.

To make fitting easier for our fitting library (Scipy's *curve\_fit* function in Python), non-laser dependent values for k have been obtained from literature [9], and kept fixed during fitting:

- $k_m = (186.12 \cdot 10^{-9})^{-1}\text{s}^{-1}$
- $k_n = (14.98 \cdot 10^{-9})^{-1}\text{s}^{-1}$
- $k_r = (14 \cdot 10^{-9})^{-1}\text{s}^{-1}$

These fixed parameters (which are obtained within the mentioned paper using fitting as well) reduce the to be fitted parameters from 5 to 4, and establishing a key relationships between the different parts of our fitting equation.

It's worth mentioning that we experimented with reducing the degrees of freedom to 3, by making  $k_d = 0.243 \cdot k_a$  (this ratio is taken from [9] aswell), however this made for slightly worse fit at high laser power regions, so we dropped this approach.

Remaining agnostic to the existence of the sixth state, we'll both sides of the argument. When taking our measurements at face value, we note the tendency towards zero saturation curves at high laser power, which would refute the existence of this particular state. When observing the obtained  $k_8$  values, here too we tend to the conclusion that this high energy (close to the conductance band) does not exist. When considering figure 33 in the appendix, which show saturation curves up to 80mW, we see how the saturation curve clearly tends towards zero.

On the other hand, we're not fully satisfied that our measurements, nor that our fits are authoritative. To point a few key questions to consider for future research:

- Why does the fit for 540nm show a nice non-zero value for  $k_8$ ?

- Why are the saturation curves for 555nm and 570nm not showing a lower powered saturation level (at about 5mW)?

Our educated guess is that our obtained saturation curves weren't obtained *carefully* enough, here again pointing at the fact that these saturation curves have been conducted by a manual turning of a polarizer which is attached to an optical bench, which propagates perturbations to the stage and objective. This is especially true at the initial turning of the polarizer: a relatively large acceleration is required to start the turning of the polarizer, and thus causing a large perturbation. Since the low laser power PL values (between 0mW to 5mW) are crucial for an adequate fit for  $k_a$ , which fits for the initial 'hump' of the curve. When  $k_a$  is misfitted, other parameters suffer from misfitting, especially when considering up to three fixed parameters which govern the shape of the saturation curve.

For future research, we truly recommend the installment of a low-noise motor-controlled polarizer-rotator. This would not only allow for a *full automation* of the saturation curve measurement process, but would also help immensely in reducing undermining perturbations from the macro world onto the micro world, and thus eliminating this elementary mistake in future measurements.

## 6 Conclusions

In this report, we explored NV-center behavior at high laser powers, with the purpose for verifying an hypothesized  $n_8$  state. In our measurements we conclude that this state does not exist, as we observed saturation curves tending to zero at high laser powers. Fitting curves on the theoretical 6-state models also shows a tendency of  $k_8$  to go to zero, which governs non-zero asymptotic behaviors. On certain wavelengths, in particular 555nm and 570nm, we observe non-zero asymptotic behavior. If the hypothesized  $n_8$  state exists, we admit that our measurements are simply incorrect. In fact, our setup suffers from perturbations caused by manually rotating a polarizer to vary huge laser powers from 0mW to max. To improve results, we propose a mechanized motor to turn the polarizer. Further, the 6-level state model could be revised by considering more transition states than the currently

The other part of our report focuses on experiments done to study PL dependence on applied voltage. Many measurements were conducted to this end, which reveals very noisy and inconsistent PL at 0V, after cycling back from non-zero voltages. By performing Rabi Oscillation measurements between and outside electrodes, we learned that within electrodes initialization issues occur, and thus there's an influence of voltage on the crystal lattice environment, which should be taken into account when conducting future research. In particular, we propose research into initialization procedures of an NV-center which has been subject to varying potentials.

## 7 Acknowledgements

We would like to thank Darya Menialava for guidance and graciousness through-out our experimental journey, Michael Petrov, and our promotor Miloš Nesladek for lending us the space to conduct experiments on our pace.

## References

- [1] Appl. Phys. Lett. 120, 162402 (2022); <https://doi.org/10.1063/5.0079667>
- [2] Gali, Ádám. "Ab initio theory of the nitrogen-vacancy center in diamond" Nanophotonics, vol. 8, no. 11, 2019, pp. 1907-1943. <https://doi.org/10.1515/nanoph-2019-0154>
- [3] Barbiero, M., Castelletto, S., Gan, X. et al. Spin-manipulated nanoscopy for single nitrogen-vacancy center localizations in nanodiamonds. Light Sci Appl 6, e17085 (2017). <https://doi.org/10.1038/lsta.2017.85>
- [4] Thiering, G., Gali, A. (2018). Ab Initio Magneto-Optical Spectrum of Group-IV Vacancy Color Centers in Diamond. Physical Review X, 8(2).<https://doi.org/10.1103/physrevx.8.021063>
- [5] Wikipedia contributors. (2023b, March 11). Nitrogen-vacancy center. Wikipedia. Retrieved March 12, 2023, from [https://en.wikipedia.org/wiki/Nitrogen-vacancy\\_center](https://en.wikipedia.org/wiki/Nitrogen-vacancy_center)
- [6] Schirhagl, R., Chang, K., Loretz, M., Degen, C. L. (2014). Nitrogen-Vacancy Centers in Diamond: Nanoscale Sensors for Physics and Biology. Annual Review of Physical Chemistry, 65(1), 83–105. <https://doi.org/10.1146/annurev-physchem-040513-103659>
- [7] Rondin, L., Tetienne, J., Hingant, T., Roch, J., Maletinsky, P., Jacques, V. (2013). Magnetometry with nitrogen-vacancy defects in diamond. Reports on Progress in Physics, 77(5), 056503. <https://doi.org/10.1088/0034-4885/77/5/056503>
- [8] Mark Fox, Quantum optics an introduction
- [9] D. Wirtitsch, G. Wachter, S. Reisenbauer, M. Gulka, V. Ivády, F. Jelezko, A. Gali, M. Nesladek, M. Trupke (2023) Exploiting ionization dynamics in the nitrogen vacancy center for rapid, high-contrast spin, and charge state initialization, *PHYSICAL REVIEW RESEARCH*, 5, 013014
- [10] Density of events paper.pdf, [https://github.com/adamblvck/QuantumUSB-Research/blob/master/resources/onTopic/Density%20of%20events%20paper%20\(1\).pdf](https://github.com/adamblvck/QuantumUSB-Research/blob/master/resources/onTopic/Density%20of%20events%20paper%20(1).pdf)
- [11] state 8.pdf, <https://github.com/adamblvck/QuantumUSB-Research/blob/master/resources/onTopic/state%208.pdf>
- [12] Wikipedia contributors. (2023). Harmonic mean. Wikipedia. [https://en.wikipedia.org/wiki/Harmonic\\_mean](https://en.wikipedia.org/wiki/Harmonic_mean)
- [13] Wikipedia contributors. (2023b). Confocal microscopy. Wikipedia. [https://en.wikipedia.org/wiki/Confocal\\_microscopy](https://en.wikipedia.org/wiki/Confocal_microscopy)

## 8 Appendix

#213 NV-Center - Smoothed Voltage Sweep at and around resonant mWave freqs- @535nm

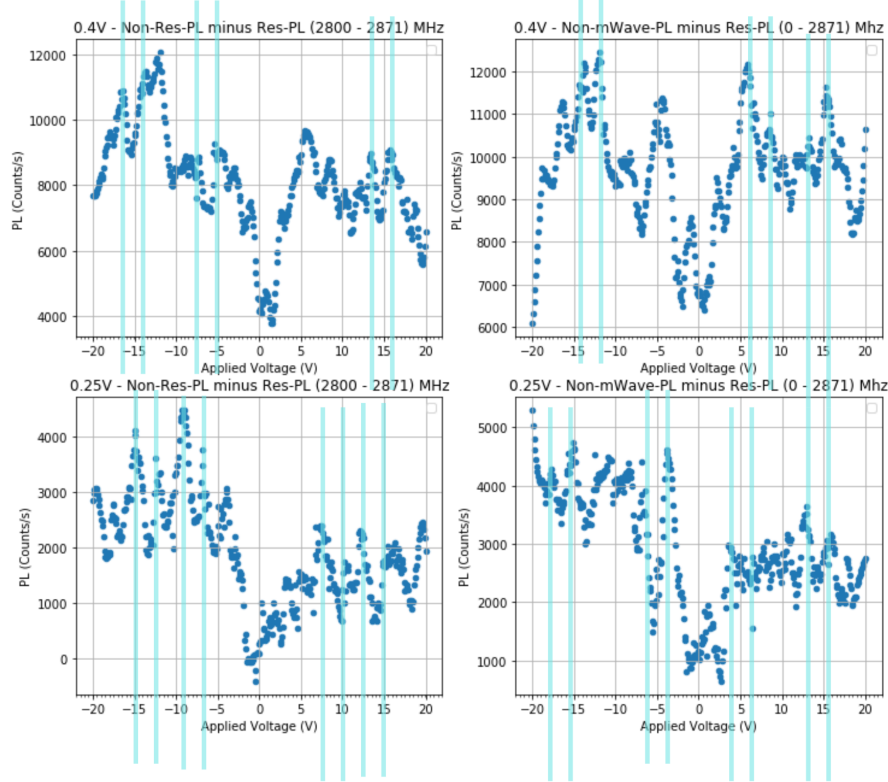


Figure 28: PL difference between resonant and non-resonant frequencies at varying voltage sweeps. Periodicity patterns are highlighted

#213 NV-Center - Smoothed Voltage Sweep at and around resonant mWave freqs- @535nm

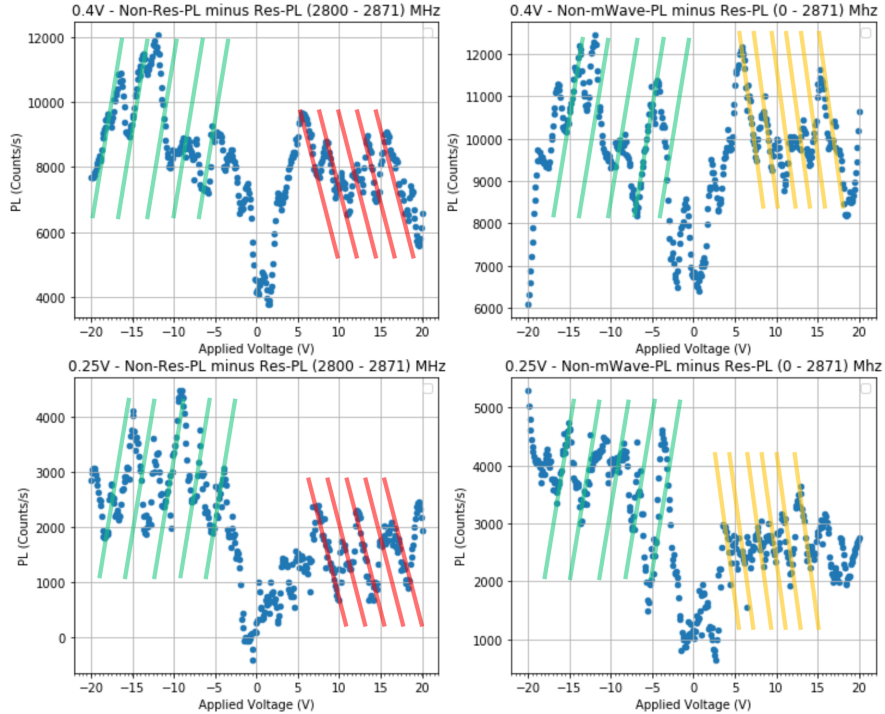


Figure 29: PL difference between resonant and non-resonant frequencies at varying voltage sweeps. Sawtooth patterns are highlighted

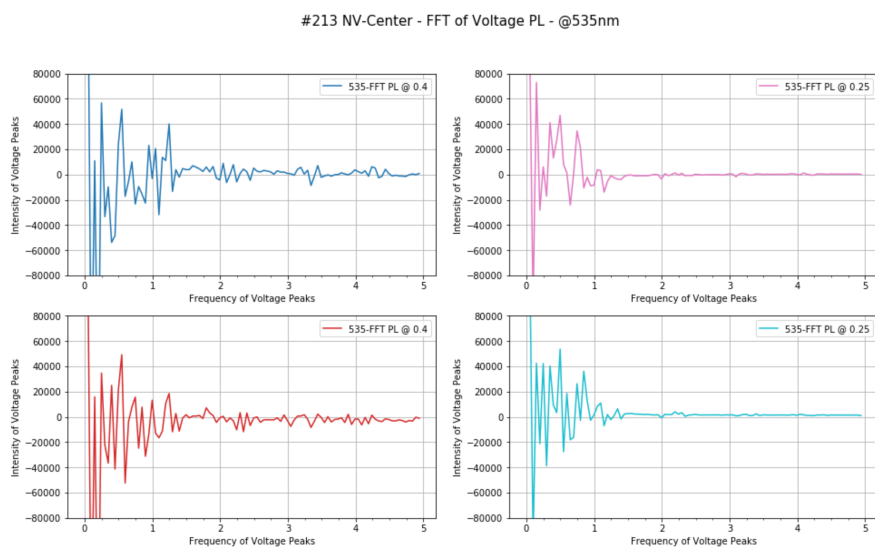


Figure 30: Respective FFTs of voltage frequencies of PL count differences in figure 28, in an attempt to notice recurring frequencies.

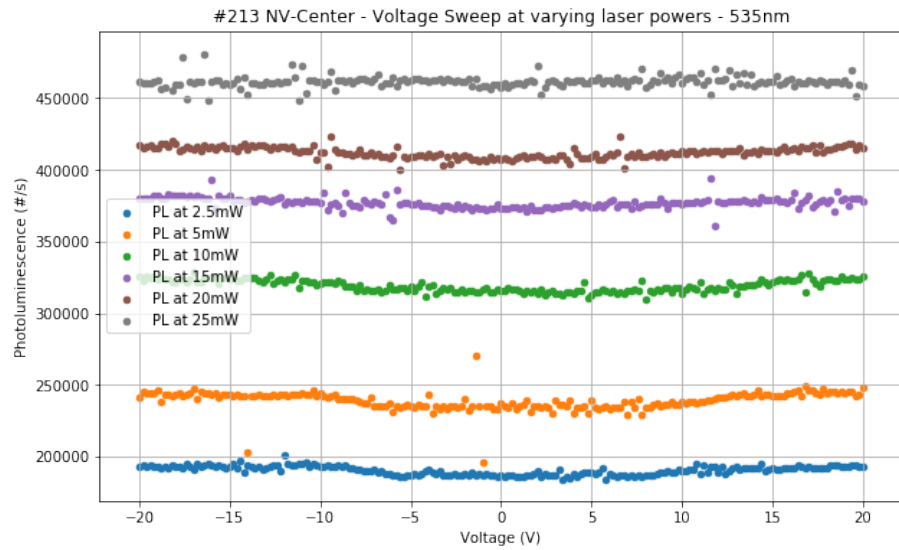


Figure 31: Point of Interest - seeking a laser power at which voltage does not make PL change

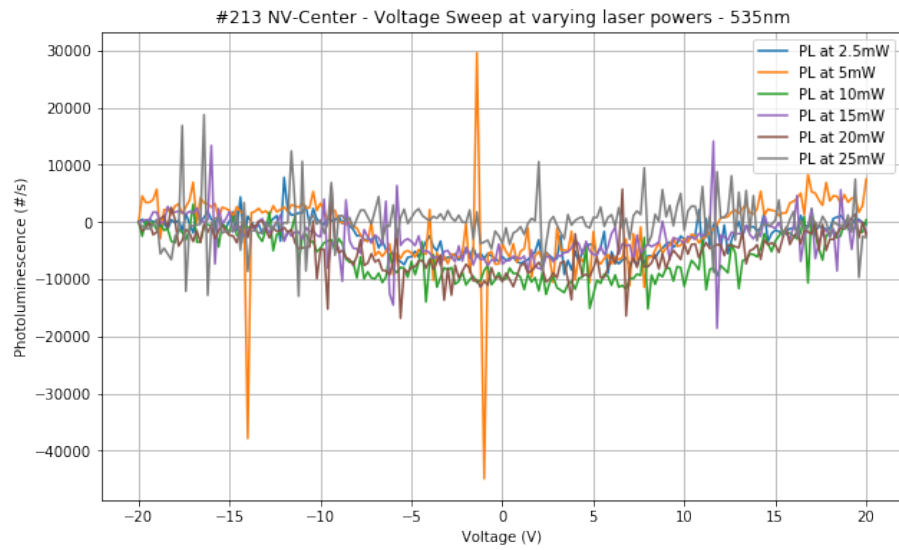


Figure 32: Point of Interest - normalized version of figure 31 as to showcase the relative contrasts for each laser power

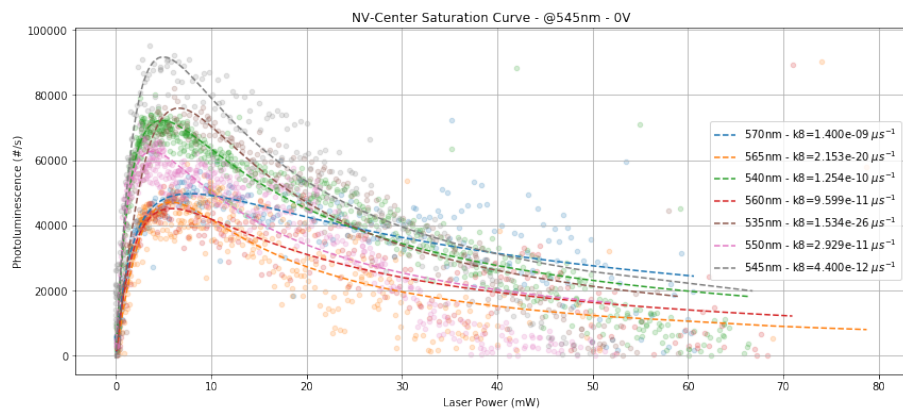


Figure 33: Saturation curves at different wavelength, fitted assuming the existence of a 8th state - done with 80mW max